

8-2018

Design of Meta-material Tank Track System with Experimental Testing and Sensitivity Analysis of Additively Manufactured Meta-material Backer Pads

Samuel J. Franklin

Clemson University, frankl6@g.clemson.edu

Follow this and additional works at: https://tigerprints.clemson.edu/all_theses

Recommended Citation

Franklin, Samuel J., "Design of Meta-material Tank Track System with Experimental Testing and Sensitivity Analysis of Additively Manufactured Meta-material Backer Pads" (2018). *All Theses*. 2947.

https://tigerprints.clemson.edu/all_theses/2947

This Thesis is brought to you for free and open access by the Theses at TigerPrints. It has been accepted for inclusion in All Theses by an authorized administrator of TigerPrints. For more information, please contact kokeefe@clemson.edu.

DESIGN OF META-MATERIAL TANK TRACK SYSTEM WITH EXPERIMENTAL
TESTING AND SENSITIVITY ANALYSIS OF ADDITIVELY MANUFACTURED
META-MATERIAL BACKER PADS

A Thesis
Presented to
the Graduate School of
Clemson University

In Partial Fulfillment
of the Requirements for the Degree
Master of Science
Mechanical Engineering

by
Samuel J. Franklin IV
August 2018

Accepted by:
Dr. Georges Fadel, Committee Chair
Dr. Nicole Coutris
Dr. Gang Li

ABSTRACT

Operational wear and hysteretic heat loss frequently affect the rubber components of the M1 Abrams main battle tank, leading to deterioration of the material and laborious replace and repair efforts in tactical situations. In previous work at Clemson University, meta-material backer pads had been designed and optimized using the Unit Cell Synthesis method and the Modified Unit Cell Synthesis method to match the characteristic deformation behavior of current elastomer backer pads on the M1 Abrams battle tank. In this case, a meta-material is a periodic, unit cell based, material that exhibits global mechanical properties that differ from the mechanical properties of the constitutive material. After successful optimization results were obtained, physical parts were manufactured using an Electron Beam Melting additive manufacturing process and a Ti-6Al-4V powder, however the behavior of the physical pads was never tested. The work in this research begins here, with the experimental testing and performance comparison of the titanium backer pads against the respective finite element model. Using compressive and high cycle fatigue testing, the behavior of one backer pad was observed, showing a desired nonlinear behavior but larger than expected strain values. Fatigue testing, in turn, resulted in a critical failure prior to meeting the desired and expected number of cycles. To search for causation for these discrepancies, three potential sources for performance deviation were identified through literature and FE model review. A sensitivity analysis was employed to analyze the influence of manufacturing tolerances and material property variation on final performance, which showed significant performance error could be

feasibly expected. In tandem with testing, expressed interest in replacing additional rubber track system components led to the design and optimization of a meta-material system. Using MUCS methodology, a circular meta-material for use on the road wheel was designed and optimized. Inadequate results encouraged the introduction of layer multipliers. The multipliers altered the design space and provided several significantly improved design options to choose from. The system design was then carried out, utilizing both a single level and multi-level optimization approach to compare against one another, based on several criteria. Finally, research questions are answered, conclusions are discussed, and the path to future work is provided.

DEDICATION

To my family and friends for their continued love and support and to Clemson University for the incredible knowledge and experience it has given me. Go Tigers!

ACKNOWLEDGMENTS

First and foremost, I would like to thank my family and friends for their unwavering support, not only in these two years at Clemson, but the many years prior. Without the emotional and financial support, these accomplishments would have remained unfulfilled dreams. The buck stops here, finally.

To Dr. Fadel: I cannot thank you enough for providing me with an opportunity to conduct this challenging, yet exciting, research. Your belief, guidance, and, most importantly, patience taught me more than any 8000 level class I took in these past two years. To Dr. Li and Dr. Coutris, your attention to detail and poignant questioning kept me focused and thorough in my work and methodology, and I hope the retirement wasn't because of me. To Dr. Summers, thank you for taking a chance on a small school physics major with a passion to be a Tiger and engineer. You challenged me upon acceptance to prove that undergrads like myself can succeed when thrown into the fire.

A big thanks goes to the sponsors of my project, the US Army ARC and TARDEC for providing the continued funding for me to pursue this research project. I would also like to thank Mike Honaker and Bill Vanslembrouck at GDLS Warren. Your guidance and input over the last year has been great. Lastly, I would like to thank ESTECO and Apurva Gokahle, without whom I may have been stuck right in front of the finish line forever.

To Dr. Rulison: Without your support and commitment to helping me overcome two years of physics requirements in only two semesters, graduate school would not have been a possibility. The countless hours of advising and independent study lectures don't

seem all that bad looking back and I wouldn't want the path to have unfolded any other way.

To my labmates: Your knowledge and friendship made life as a GRA two of the most impactful years of my life. From movie nights to homework help to conversation in the office, there are more than a few problems that I may not have overcome if it hadn't been for your willingness to help a friend in need. And let's not forget the time we took over Tampa for the single greatest football game there ever was! **35-31!!**

To Miranda: Long distance was miserable. Let's agree not to do that ever again. You're the best and I love you!

To Eric: Danke, mein freund.

TABLE OF CONTENTS

	Page
ABSTRACT	ii
DEDICATION	iv
ACKNOWLEDGMENTS	v
TABLE OF CONTENTS	viii
LIST OF TABLES	xi
LIST OF FIGURES	xii
CHAPTER 1. INTRODUCTION	1
1.1. THE MODIFIED UNIT CELL SYNTHESIS METHOD	1
1.2. INITIAL BACKER PAD CASE STUDY	5
1.3. PRELIMINARY RESEARCH QUESTIONS.....	9
1.4. THESIS ORGANIZATION	11
CHAPTER 2. EXPERIMENTAL VALIDATION AND DISCREPANCY INVESTIGATION	13
2.1. QUASI-STATIC COMPRESSION TESTING	13
2.2. HIGH CYCLE FATIGUE TESTING.....	15
2.3. IDENTIFYING POTENTIAL SOURCES OF DISCREPANCIES	18
2.3.1. MATERIAL PROPERTIES VARIANCES	20
2.3.2. GEOMETRIC DIMENSIONAL VARIANCES	22

2.3.3.	ACCURATE MODELLING OF BOUNDARY CONDITIONS.....	24
2.4.	SENSITIVITY ANALYSIS OF POTENTIAL MATERIAL AND DIMENSIONAL INACCURACIES	26
2.4.1.	DESIGN OF EXPERIMENT METHODOLOGY	27
2.4.2.	SENSITIVITY ANALYSIS OF OPTIMIZED PAD	29
2.4.3.	INTERACTION PLOTS	33
2.4.4.	SIGNIFICANCE OF MATERIAL PROPERTY VARIANCES	36
2.5.	RESULTS AND DISCUSSION.....	38
2.6.	PROPOSED IMPLEMENTATION OF SENSITIVITY ANALYSES IN MUCS METHOD ..	39
 CHAPTER 3. BEHAVIORAL INVESTIGATION AND OPTIMIZATION OF CIRCULAR META-MATERIAL FOR TANK ROAD WHEEL.....		41
3.1.	META-MATERIAL DESIGN REQUIREMENTS.....	41
3.1.1.	UC SELECTION FOR POLAR MAPPING	42
3.1.2.	DESIGN VARIABLE MODIFICATIONS	44
3.1.3.	META-BAND DESIGN FOR MULTI-OBJECTIVE OPTIMIZATION	45
3.2.	INITIAL META-BAND OPTIMIZATION	47
3.2.1.	ABAQUS PARAMETERIZATION & WORKFLOW	47
3.2.2.	RESULTS AND DISCUSSION	49
3.3.	INTRODUCTION OF SIZE FACTORS FOR INCREASED NONLINEARITY.....	50
3.3.1.	APPLICATION OF SIZE FACTORS.....	51
3.3.2.	INITIAL ASSUMPTION	52
3.4.	RE-OPTIMIZATION OF META-BAND WITH SIZE FACTORS.....	54

3.4.1.	ADJUSTED PARAMETERIZATION AND OPTIMIZER WORKFLOW	55
3.4.2.	OPTIMIZATION RESULTS AND DISCUSSION	56
3.5.	CONCLUSIONS AND DISCUSSION	62
CHAPTER 4. MULTI-LEVEL OPTIMIZATION OF TANK TRACK SYSTEM		
METAMATERIALS		64
4.1.	SYSTEM APPROACH	64
4.1.1.	SINGLE AND MULTI-LEVEL OPTIMIZATION	64
4.1.2.	TARGET GATHERING	66
4.2.	MULTI-LEVEL OPTIMIZATION PROCEDURE	70
4.2.1.	STEP 1: PAD REOPTIMIZATION	71
4.2.2.	STEP 2: BI-LEVEL ITERATIVE LOOP	72
4.2.3.	CONSIDERATIONS FOR OPTIMIZATION IN MODEFRONTIER	73
4.3.	CANTI-DUO BACKER PAD - RUBBER WHEEL OPTIMIZATION	74
4.4.	MULTI-LEVEL OPTIMIZATION RESULTS	79
4.5.	SINGLE LEVEL OPTIMIZATION SET-UP & RESULTS	84
4.6.	COMPARISON OF RESULTS AND DISCUSSION	91
CHAPTER 5. CONCLUSIONS AND FUTURE WORK		95
5.1.	CONCLUSIONS	95
5.2.	FUTURE WORK	98
5.2.1.	BACKER PAD EXPERIMENTAL TESTING	98
5.2.2.	SENSITIVITY ANALYSIS FOR META-MATERIAL SYSTEM	99

5.2.3.	EXPANDED OPTIMIZATION OF META-MATERIAL SYSTEM	100
5.2.4.	MULTI-LEVEL OPTIMIZATION.....	101
REFERENCES.....		103

LIST OF TABLES

	Page
Table 1.1 Backer Pad Case Study Optimization Parameters	8
Table 1.2 Backer Pad Case Study Optimization Results for Three UC Configurations	9
Table 2.1 Importance Value Equations and Definitions	28
Table 2.2 Orthogonal Array Table for L16 (215) Taguchi Array	31
Table 2.3 Significance Values for Design Parameters of Backer Pad.....	32
Table 2.4 Parameter Values for High and Low Responses	39
Table 3.1 Initial Meta-band Design Variables & Material Properties.....	47
Table 3.2 Optimal Design Parameters for Meta-band w/ Unorganized SF	61
Table 4.1 Target Strains for Track System Rubber Components	70
Table 4.2 Backer Pad Reoptimization Objectives & Constraints	76
Table 4.3 Optimal Design Parameters for Canti-Duo Backer Pad.....	79
Table 4.4 Multi-Level Optimization Objectives, Constraints, & Termination Criteria ...	80
Table 4.5 Multi-Level Optimization Subsystem & Global Strain Values.....	81
Table 4.6 Multi-Level Optimization Optimal Design Variables.....	84
Table 4.7 Single Level Optimization Objectives & Constraints	87
Table 4.8 Single Level Optimization Subsystem and Global Strain Values	89
Table 4.9 Final Design Parameters from Single Level Meta-material Optimization.....	91

LIST OF FIGURES

	Page
Figure 1.1 Representation of M1 Abrams Single Track Linkage	1
Figure 1.2 Progression of Backer Pad Deterioration due to Hysteretic Heat Loss	2
Figure 1.3 Original and Modified Unit Cell Synthesis Method. Green box indicates the modification	5
Figure 1.4 (Top Left) Canti-Duo (Top Right) Canti-Oval Bi-Parallel (Bottom) Canti-Oval [8].....	7
Figure 1.5 Heat Map of M1 Track System	10
Figure 2.1 Experimental Set-up for Compressive Testing of Backer Pad.....	14
Figure 2.2 Experimental Response of Canti-Oval Meta-material.....	14
Figure 2.3 Experimental and Expected Responses of the Metamaterial Pad	15
Figure 2.4 Experimental Set-up for High Cycle Fatigue Testing of Backer Pad.....	16
Figure 2.5 Chart of Hysteretic Loops from High Cycle Fatigue Testing	18
Figure 2.6 Original Boundary Conditions for the Backer Pad FE Model	24
Figure 2.7 Modified Boundary Conditions for the Backer Pad FE Model.....	25
Figure 2.8 Changes in Mechanical Response due to Boundary Condition Modification	26
Figure 2.9 Effects of Most and Least Significant Parameters on Pad Behavior	33
Figure 2.10 Unit Cell W and CB Thickness Interaction Plot	34
Figure 2.11 Potential Effects of Printing Tolerances on Backer Pad Performance	36
Figure 2.12 Effects of Material Property Changes of Backer Pad Behavior	37
Figure 2.13 Upper and Lower Bounds of Deformation Behavior for Metamaterial Pad.	39
Figure 3.1 Target Mechanical Behavior for Initial Meta-band Optimization.....	43
Figure 3.2 General Deformation Behavior of Canti-Duo UC Design.....	43

Figure 3.3 Canti-Duo Unit Cell Design.....	44
Figure 3.4 Modified Canti-Duo UC for Meta-Band	45
Figure 3.5 Tessellated Canti-Duo UC for Meta-Band.....	46
Figure 3.6 Results of Initial Canti-Duo Meta-band Optimization	49
Figure 3.7 Size Factors Applied to a Canti-Duo UC.....	52
Figure 3.8 Representation of Gradient Based Size Factor Organization.....	54
Figure 3.9 Meta-Band Optimization w/ Unorganized SF Design Summary Chart	56
Figure 3.10 Mechanical Response of Meta-Band w/ Unorganized SF & No SF	57
Figure 3.11 Meta-Band w. Unorganized SF Optimization Design Summary Chart.....	58
Figure 3.12 Meta-Band w/ Organized SF Optimization Design Chart	59
Figure 3.13 Mechanical Response of Meta-Band w/Unorganized SF	60
Figure 3.14 Layer by Layer Size Factor Distribution For Meta-band w/ Unorganized SF	61
Figure 3.15 Mechanical Response of Meta-Band w/ Organized SF, Unorganized SF, and no SF.....	62
Figure 4.1 Comparison of Single and Multi-Level Optimization Methods for Metamaterial System	66
Figure 4.2 Representation of Rubber-Rubber Target Deformation	67
Figure 4.3 (Left) Single Level Optimization Target Deformation Curve. (Right) Multi-Level Optimization	67
Figure 4.4 (Left) Meta-Band on Rubber Pad. (Right) Rubber-lined Wheel on Meta-Pad	68
Figure 4.5 (Top Left) Pad Response in Rubber-Rubber. (Top Right) Wheel Response in Rubber-Rubber Model.	69
Figure 4.6 Diagram of Multi-Level Optimization Process	70
Figure 4.7 Step 1: Pad Reoptimization for Multi-Level Optimization.....	71
Figure 4.8 Step 2: Iterative Loop for Meta-material System Optimization.....	72
Figure 4.9 ModeFRONTIER Loop Diagram for Multi-Level Optimization.....	74

Figure 4.10	Updated ModeFRONTIER Loop Diagram for Multi-Level Optimization...	74
Figure 4.11	FE Model of Canti-Duo Pad and Original Track System Road Wheel	76
Figure 4.12	Canti-Duo Backer Pad & Rubber Wheel Design Summary Chart	77
Figure 4.13	Canti-Duo Backer Pad & Rubber Wheel Design Chart.....	77
Figure 4.14	Mechanical Response of Reoptimized Canti-Duo Pad.....	78
Figure 4.15	Profile of Canti-Duo Pad Final Design	78
Figure 4.16	Canti-Duo Backer Pad Distribution of Size Factors.....	79
Figure 4.17	Bi-Level Optimization Subsystem Mechanical Responses	82
Figure 4.18	Bi-Level Optimization Global Mechanical Response	83
Figure 4.19	Multi-Level Optimization Size Factor Distribution	84
Figure 4.20	Measured Displacements of Single Level Optimization	85
Figure 4.21	Target Response of Rubber-Rubber Track System	86
Figure 4.22	Design Summary Chart of Single Level Meta-material Optimization	88
Figure 4.23	Design Objective Scatter Chart of Single Level Meta-material Optimization	88
Figure 4.24	Single Level Optimization Mechanical Responses of Meta-material Subsystems.....	89
Figure 4.25	Single Level Optimization Mechanical Response of Meta-material System	90
Figure 4.26	Layer by Layer Breakdown of Meta-material Size Factors	91

CHAPTER 1. INTRODUCTION

1.1. The Modified Unit Cell Synthesis Method

The M1 Abrams battle tank is employed by the US Army in a variety of tactical and peace keeping operations across the world and in various urban and remote environments. Currently, the tank utilizes the T158LL track pad to provide traction, sound dampening, and road surface protection during regular operation [1]. This is possible because of the high strains experienced at low stress levels, followed by a nonlinear stiffening as loads increase. These track pads are used on both the ground side and interior side of the steel track, which can be seen in Figure 1.1.

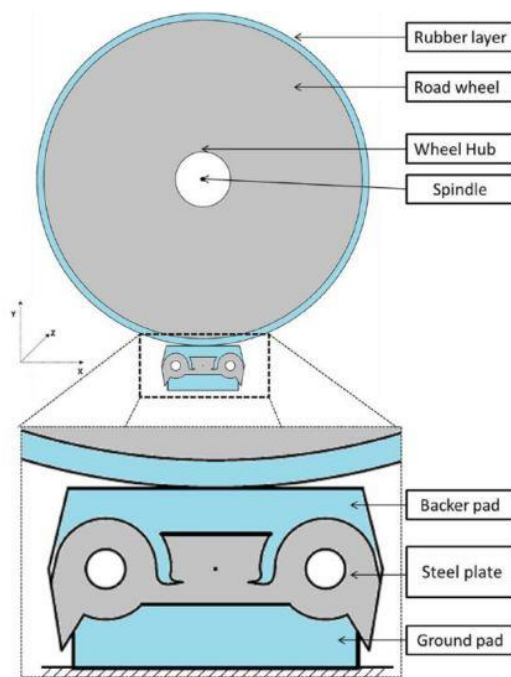


Figure 1.1 Representation of M1 Abrams Single Track Linkage [2]

The T158LL pad is made of a Styrene-Butadiene Rubber (SBR), filled with black carbon reinforcements meant to improve overall pad strength and abrasion resistance [3].

Despite these considerations for improved product life, the pads experience occasional failure, typically through blowouts, which occur after sustained high-speed operation. The rapid cyclic compression leads to overheating and hysteretic losses, resulting in temperature increases of more than 300°C [4]. Eventually, the pads begin to crack, break apart, and subsequently deteriorate, an example of which can be seen in Figure 1.2. The costs associated with replacing these pads are high. Not only does the track need to be removed, but each damaged link must be replaced with a new one. Despite the rubber being a relatively inexpensive material, the current manufacturers details that in order to replace the damaged component, the entire linkage must be removed and scrapped. This drives up the overall cost associated with these repairs, as the steel linkage coupled with the rubber is substantially more expensive.[3].



Figure 1.2 Progression of Backer Pad Deterioration due to Hysteretic Heat Loss [5]

With these known limitations for the elastomer pads, a new material was sought to achieve favorable high compliance, while reducing or eliminating the hysteretic heat loss and subsequent deterioration. Initial attempts to address this need, utilizing topological optimization, were unfruitful. Traditional topological optimization as we implemented it,

lacked the ability to consistently and effectively curve match the designed material's mechanical response, especially when considering the boundary conditions and manufacturing considerations [6]. Topology optimization generally searches for a design based on a desired compliance or on material properties of the global structure, which are fixed across the entire loading range. The limitations of topology optimization for these cellular materials are discussed further in [6]

To address these limitations and the need for viable materials for nonlinear applications, the implementation of cellular structures, comprised of a linear elastic constitutive material, was introduced as an exploratory option. With a material made from a linear elastic base, such as metal, hysteretic heat buildup is not a significant issue. Additionally, some of these materials can have favorable elastic modulus-to-yield stress ratios, providing the cellular material with the ability to undergo large deflections while remaining within the elastic range. From a manufacturing standpoint, these cellular designs were enabled through the expansion of additive manufacturing technologies, using metal powders and high powered laser or energy beam melting for instance to construct previously unobtainable designs.

The first several steps in obtaining these cellular materials, or meta-materials as referred to in [7], revolve around the design of a unit cell (UC). These UCs are the building blocks of the meta-materials and constructed of both Elemental Functional Geometries (EFGs) and Elemental Support Geometries (ESGs). These geometries dictate the behavior of the UC under loading and how the load is transferred from one layer of cells to the other, after tessellation [7]. When these unit cells are tessellated, they form a representative

volume element (RVE). These RVEs are classified in two cases, the first being a material where the size of the global structure is much larger than the size of the base UC. This scenario is particularly useful when boundary conditions are unknown or approximated. The second class of RVE is a material comprised of a relatively small number of UCs in the x and y directions. These type of materials are used when the size of the target structure is a driving influence and the number of UCs in the material are restricted. These particular RVEs are particularly susceptible to the effects of boundary conditions for the global structure [7].

Implementing these new characteristics, a preliminary and updated design methodology, dubbed the “Unit Cell Synthesis Method” and “Modified Unit Cell Synthesis Method” respectively, were created for the systematic design and optimization of unit cell based cellular materials for nonlinear applications [6][8]. Figure 1.3 shows the steps of the Modified Unit Cell Synthesis Method, and more information on the specifics of the steps can be found in the theses presented by Kulkarni [7] and Satterfield [9]. These ‘metamaterials’ are designed from a repository of beam elements, placed in various combinations of series and parallel arrangements to achieve a general pattern of behavior. The arrangements are then subjected to a dimensional optimization, narrowing the material performance to best match the target response.

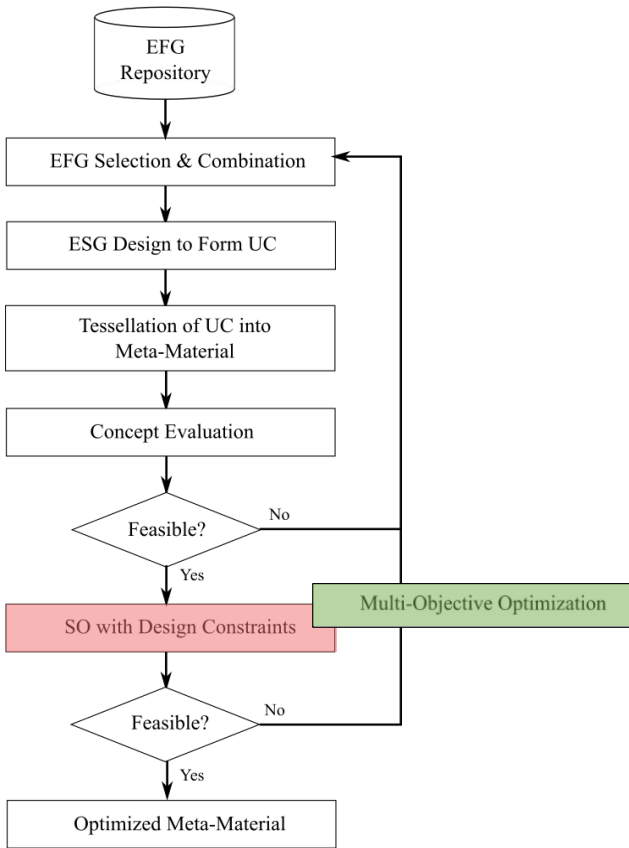


Figure 1.3 Original and Modified Unit Cell Synthesis Method. Green box indicates the modification [8]

The work presented in this thesis looks to wrap up the initial investigation of replacement metamaterials for the rubber elastomer backer pads, while also beginning a larger investigation into the behavior of the track system and how similar metamaterials could be implemented to replace the rubber components.

1.2. Initial Backer Pad Case Study

With a systematic methodology created for the design of these nonlinear metamaterials, a case study was carried out to generate a feasible replacement material specifically for the rubber backer pads of the M1 tank. Using a model of the original backer pad material under compression, the favorable response of the rubber was documented for

use as a target in the material design. The nonlinear behavior of the elastomer pads provides stiffening as loading increases, an important characteristic that needed to be met as initial beam element selections were being made. As outlined in the Modified Unit Cell Synthesis method, the first steps are to select and arrange the structural building blocks for the unit cell (UC) for eventual tessellation.

By identifying the general behavior trends of various individual and combined elements, the determination of feasible unit cell designs is expedited. From there, exploratory designs of experiments were used to help judge feasibility for optimization. In this particular case study, three unique cell configurations were determined to be feasible options for expanded multiobjective optimization, each created and tested after the prior returned inadequate results. The first cellular configuration, dubbed ‘canti-duo’, is the most simplistic of the cells and uses two cantilever beams attached to elemental support geometries (ESG) structures, which are the red members in Figure 1.4.. The second unit cell configuration, “canti-oval bi-parallel” combines the cantilever beam with an oval beam. This particular configuration highlights one of the unique characteristics of the Modified UCS method, which is the utilization of beam element combinations, in both series or parallel, similar to how circuit elements are combined for particular compounding effects. For the second cell configuration, a cantilever and oval beam are placed in parallel with each other, described by their corresponding circuit diagram in Figure 1.4, creating a combination of elements that also provides the general desired mechanical behavior. Lastly, the third unit cell configuration (canti-oval) utilizes the same individual beam elements of the ‘canti-oval bi-parallel’ UC, with cantilever and oval beams combined in

series, rather than in parallel. All three of these UC configurations can be seen in Figure 1.4.

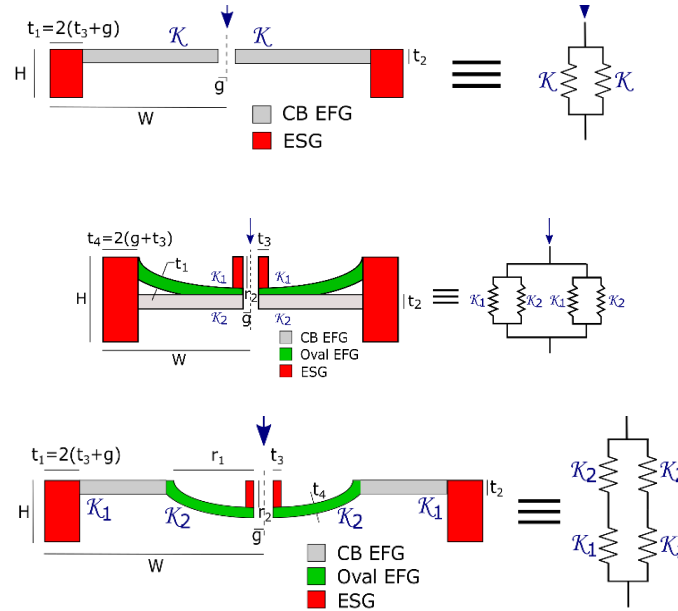


Figure 1.4 (Top Left) Canti-Duo (Top Right) Canti-Oval Bi-Parallel (Bottom) Canti-Oval [8]

Once feasible design solutions are obtained from UC construction, the next step in the case study, and the greater Modified UCS method, is to prepare the multiobjective optimization for submission. In order to use the optimization software modeFRONTIER (mF), the FE models are converted into parameterized python files, capable of manipulation by the built-in scheduling process. Using a Uniform Latin Hypercube to establish the initial DOE, the NSGA-II search algorithm was chosen to explore the design space and evaluate up to 1000 possible solutions within the predefined limits of the parameters. As for the two design objectives, the first is to minimize the sum of the squares of the errors between the target and predicted strains and the second is to minimize the maximum stress the design is calculated to incur. Both of these design objectives are

accompanied by respective constraints, used to determine the objective results that are acceptable. The details of the optimization are shown in Table 1.1.

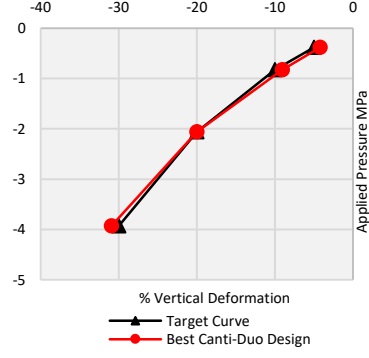
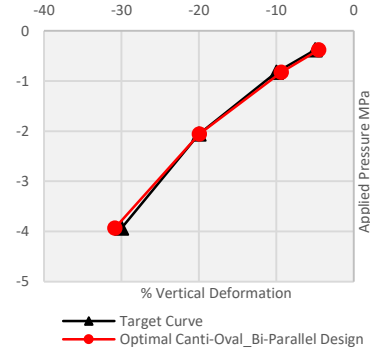
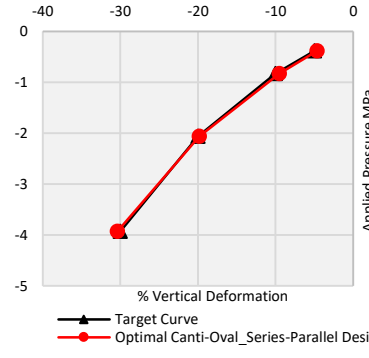
Table 1.1 Backer Pad Case Study Optimization Parameters

Description	Value
Search Algorithm used for Multi-Objective Optimization	NSGA-II
Objective Expressions [8]	$\min Strain_{Error} : f_1 = \sum_{i=1}^4 (\varepsilon_i^t - \varepsilon_i^c)^2$ $\min Max_Stress : f_2 = \max \sigma_{Von-Mises}$
Variable Equations [8]	$Meta_Strain = \frac{\delta_y}{H_{Total}} * 100\%$
Objective Constraints [8]	$Strain_{Error} \leq 2.5E^{-4}$ $Max_Stress \leq 950 MPa$

The first design tested (canti-duo) returned roughly 1% of the designs as feasible, meaning they satisfied both constraints. However, the max stress incurred was on the high side of the spectrum, and when combined with the low percentage of parameter solutions, the design was rejected as an acceptable choice. The second of the designs (canti-oval bi-parallel) optimal solution achieved a lower value for both of the optimization objectives and returned more than 27% feasible design points. Manufacturing limitations, unfortunately, would prevent the set of optimal designs from being printed, with multiple final design parameters falling at or below 0.5mm. These values are close to or less than the known manufacturing tolerance of some additive manufacturing processes, thus forcing the designers to repeat the design process and test the third option, the ‘canti-oval’ design.

After optimization, this third design returned 65% feasible design points and a most optimal design that boasted both the lowest stress and strain error values of the three cases. Analyzing the output parameters confirmed that the design was manufacturable, providing a viable meta-material design. The final objective values and mechanical behavior compared to the target are provided in Table 1.2

Table 1.2 Backer Pad Case Study Optimization Results for Three UC Configurations

Canti-Duo [8]	Canti-Oval Bi-Parallel [8]	Canti-Oval [8]
Strain Error = 2.38E-4 Max Stress = 933 MPa	Strain Error = 1.35E-4 Max Stress = 894 MPa	Strain Error = 4.45E-5 Max Stress = 834 MPa
		

1.3. Preliminary Research Questions

With a backer pad design successfully obtained via the Modified Unit Cell Synthesis Method, and physical parts printed and delivered, two research questions emerged for the continuation of the meta-material design investigation. The first, spurred by the need to test the printed pads, was:

RQ1. How does the mechanical behavior of the manufactured backer pads compare to the expected behavior of the FE model, both under quasi-static compression and high cycle fatigue?

This question is imperative to answer, as it would reveal the mechanical behavior of the physical parts and could validate the FE model as a predictable, manufacturable design for eventual implantation on the M1.

On the other hand, the successful creation of a theoretical meta-material model encourages the further implementation of the method. By designing additional meta-materials for the M1 Abrams track system, particularly materials that may be in contact with the backer pad or offer a tactical advantage through replacement, information on multiple material systems and designing for unique interactions could be collected. One such material is the thin rubber layer surrounding the road wheels in the track system. Like the original backer pads, the rubber layer around the road wheel provides favorable nonlinear mechanical behavior but is also susceptible to severe hysteretic heat loss and subsequent break apart, as shown in Figure 1.5, and adds more incentive to finding a viable alternative material.

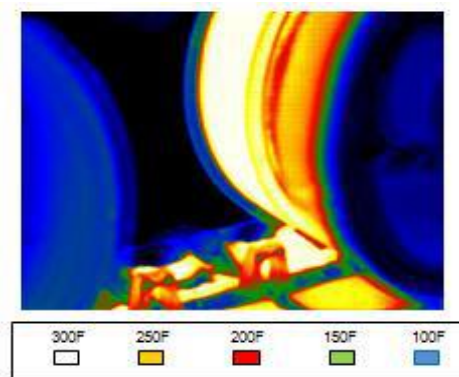


Figure 1.5 Heat Map of M1 Track System [4]

To address these several drawbacks in the current track system and to further the implementation of the Modified UCS method for meta-material design, the following research question was formulated:

RQ2. Can a system of meta-materials be designed and optimized, using the Modified Unit Cell Synthesis method, to match the target behavior of the current rubber-rubber track system?

While broad, the search for this particular answer would open the door to several more questions geared towards the specifics of the system investigation, the feasibility of designing meta-materials with a nonlinear orientation, and the implementation of a new set of design parameters that could greatly expand the capabilities of periodic cellular materials as a whole. Furthermore, these new designs would provide the opportunity for additional manufacturing and testing, aiding the cause of RQ1 and its search for performance verification outside of the theoretical realm.

1.4. Thesis Organization

The thesis is organized as follows. Chapter 1 discusses the work previously conducted with the Modified Unit Cell Synthesis Method and designing a replacement backer pad for the M1 Abrams battle tank. This chapter also covers the guiding motivation and initial research questions for the continued implementation and validation of the method. Chapter 2 looks to answer the first of the two initial research question through experimental compressive and fatigue testing of the additively manufactured backer pads. Additionally, it highlights the methodological search for discrepancy causation, after differences between the experimental and expected test results were discovered. Chapter 3

poses several new research questions in the attempt to answer the second initial question. They are answered by exploring the design and optimization of a circular meta-material for the track system road wheel, before allowing the investigation to move to the full system approach. Chapter 3 also documents the creation of ‘size factors’ as an added layer of complexity and variety in the process. Chapter 4 combines the successfully optimized “meta-band” design and a redesigned meta-material backer pad in a system of meta-materials. Using two separate optimization techniques, this section also compares the results of the optimizations to determine the ideal method for the design of these meta-material systems. Lastly, chapter 5 recaps the research questions and answers, provides conclusions of the investigation as a whole, and outlines the potential for future work and recommendations to improve further optimization efforts.

CHAPTER 2. EXPERIMENTAL VALIDATION AND DISCREPANCY INVESTIGATION

2.1. Quasi-Static Compression Testing

To ensure that the overall behavior of the designed material would closely resemble the original material both inside and outside the target range of performance, the original FE analyses considered a maximum load of 4MPa. However, for testing purposes, loading was capped at roughly 1MPa of pressure, or 22.5kN across the pad's top surface. While the metamaterial was optimized to mimic the elastomer material across the larger stress-strain relationship, performance with respect to known loads transmitted by the tank were the primary concern. The max load of 1MPa reflects the maximum pressure built up on the surface of the pads in contact with the road wheels while the tank sits statically. If the pad did not perform as desired for those loads, then performance outside of that range would be of little use. From here on, the loading will be referred to in terms of applied force (N or kN) to maintain consistency with the testing data. The 22.5kN limit also fit within the limitations of on campus testing resources, allowing for results to be obtained quickly. The experimental set-up is shown in Figure 2.1, with the meta-material pad compressed between the steel plate and base of the load frame.

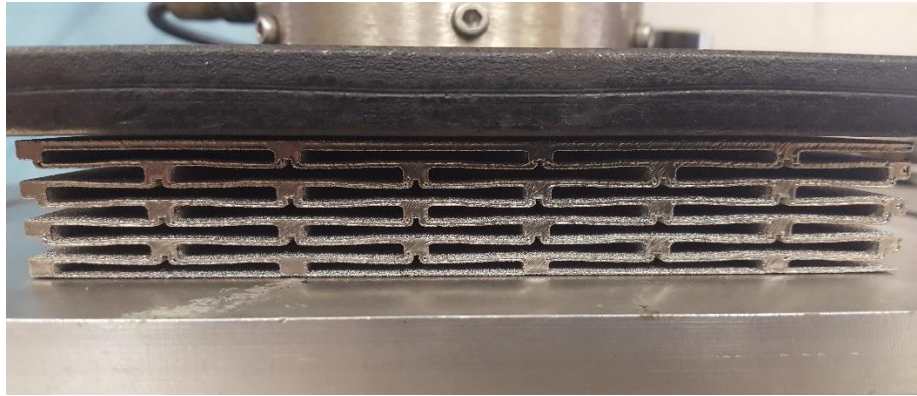


Figure 2.1 Experimental Set-up for Compressive Testing of Backer Pad

Using 22.5kN as the upper limitation of the static testing, the pad was subjected to five different loads in quasi-static compression. An Instron tabletop load frame, with a 25kN load cell and steel compression plates was used to conduct the test. The loads were applied at a uniform rate and the displacement of the load frame actuator was recorded versus time, After converting them to a percent strain for the pad, the five obtained values were plotted with respect to their corresponding stress values, as shown in Figure 2.2. In the graph, a nonlinear response can be observed, with the material showing a stiffening effect as stresses increase.

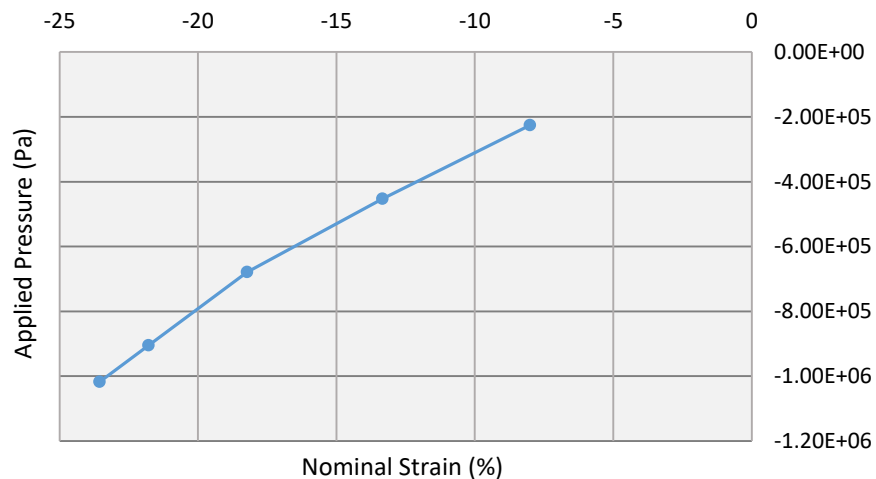


Figure 2.2 Experimental Response of Canti-Oval Meta-material

The nonlinearity observed during the experimental procedure does provide a proof of concept for the design of the pad, marking a success for the project. But, after obtaining the experimental values, it was critical to determine whether or not the observed experimental response was in accordance with the expected results produced by the FE model. In order to accurately compare the two curves, the original model was rerun at five comparable load increments, providing a second curve. The two curves were then plotted against each other, as shown in Figure 2.3.

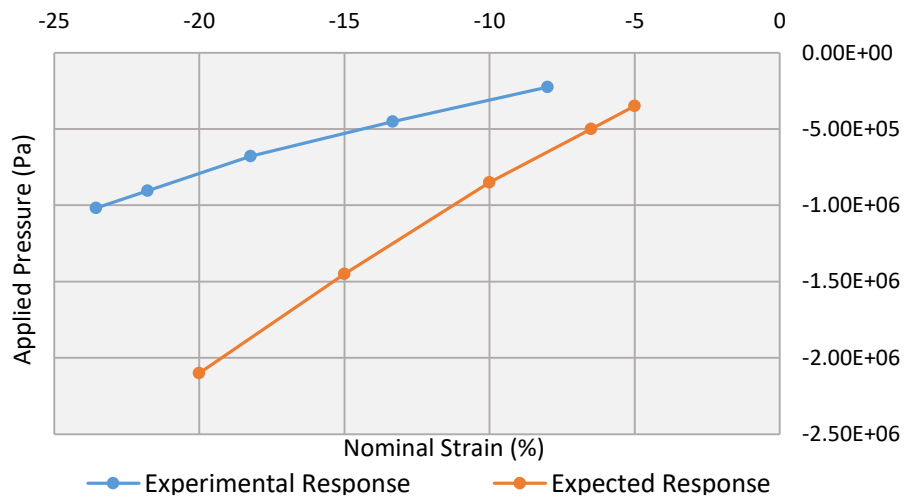


Figure 2.3 Experimental and Expected Responses of the Metamaterial Pad

As is evident from the graph, the two curves are not identical, with the physical pad exhibiting a softer response than the FE model suggests. The reasons for the large difference between expected and actual behavior needed to be investigated.

2.2. High Cycle Fatigue Testing

After the compression testing and analysis, it was decided to move forward with a high-cycle fatigue test, designed to push the pad to its breaking limits. This test would be step one in determining if the meta-material backer pad could be trusted to withstand the

punishing life on the tank. A goal of 400,000 cycles was used for the test, which had been previously estimated in the thesis of Mr. Kulkarni as an expectable expectation for 500 miles of distance traveled.

An MTS Landmark load frame was used to conduct this test, with a 100kN load cell. Two MTS compression platens were used as the attachments to apply the load, while the same 22.5kN max load was used as the upper limit of the fatigue test and a 1.125kN load was used as the lower limit. This provided the test with a load ratio of 0.05, and also ensured that the pad would always remain in some compression state, keeping it safely sandwiched between the two compression platens. Figure 2.4 shows the entire experimental set-up with the pad placed between the two platens.

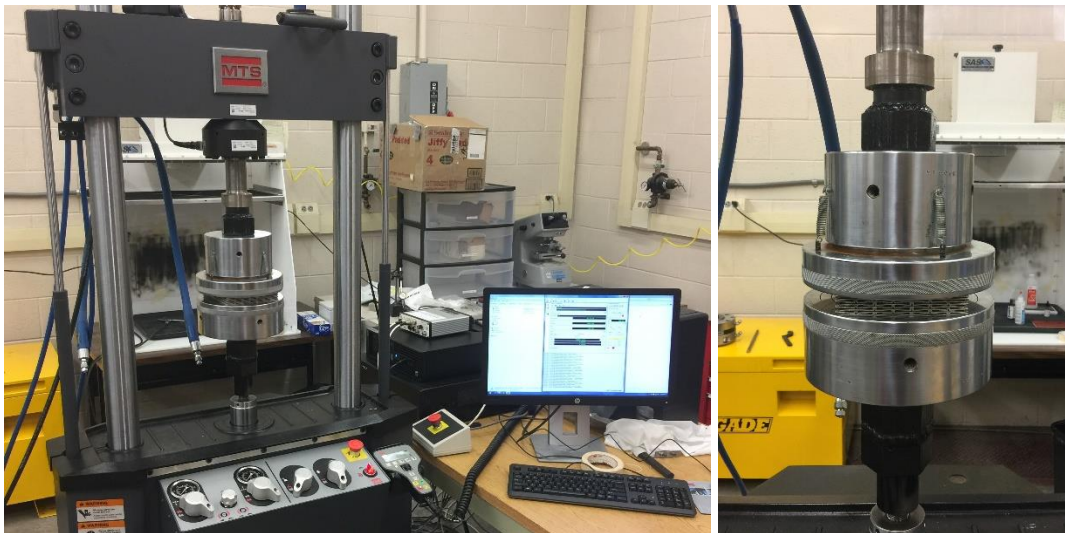


Figure 2.4 Experimental Set-up for High Cycle Fatigue Testing of Backer Pad

Lastly, a frequency needed to be determined for the test. At a speed of 45mph, the Abrams backer pads experience a load between 4 and 5 times a second. This is a high frequency for the large deformations expected from the pad, but is reflective of operating conditions. Literature also suggests that higher frequencies in fatigue testing produce

higher fatigue strengths, particularly in low stress ratio environments like the one chosen for the pad [10]. This made a strong argument for running the test at a higher end of the frequency spectrum. But other considerations suggested that a lower frequency should be selected, at least for the preliminary testing. This was in part for safety purposes, as fatigue testing at high strains had not been conducted on the particular machine, nor with these pads. Additionally, and similarly to the compression testing, if significantly positive results could not be obtained at this lower frequency, then expectation for higher frequencies would be minimal. Therefore, a frequency of 1Hz was chosen as the initial testing parameter.

Prior to testing, fatigue results from a predictive fatigue model of the pad design suggested that the pad would meet the 400,000 cycle goal at 22.5kN, and should experience infinite life at loads below 13.5kN. The fatigue model was operating under the assumption that the pad would only reach strains of about 11%, as originally optimized. But, as was evident from our static results, the pad was experiencing strains double that of the original predictions. These larger strains would undoubtedly effect the behavior of the pad in fatigue. That inclination was proven right when, after only 8,000 cycles, the pad suffered total failure at several of the critical points identified by the ANSYS model. Figure 2.5 shows the hysteretic loops of the printed backer pad at several cycle increments, up to 10,000 cycles. It is clear from the loops that a critical failure of some form occurs around the 8,000 loop mark, where displacement behaviors change drastically.

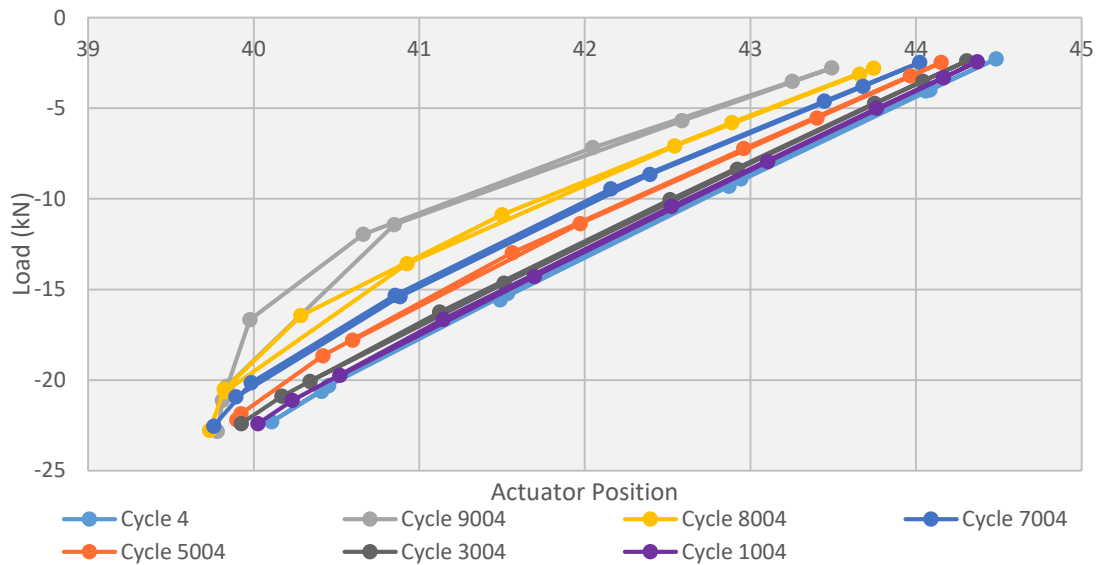


Figure 2.5 Chart of Hysteretic Loops from High Cycle Fatigue Testing

Unfortunately, due to the limited number of pads originally printed, there was only one available for testing. Because of this, it is impossible to draw any conclusions from this one test, and more tests are planned once more pads can be printed.

2.3. Identifying Potential Sources of Discrepancies

While the initial research question was successfully answered by the experimental testing of the backer pad, new concerns arose as a result. Some discrepancies between the experiment and the numerical results are not entirely unexpected, due to known variability from batch to batch or even part to part in additive manufacturing, but such a large deviation prompted the formulation of an additional research question that required answers. The question states: What potential sources for the deviation between experimental and predicted model responses can be identified, and how much effect could they impart on the system. This problem prompted the beginning of an investigation to determine causes for this discrepancy.

Without the availability of additional pads to corroborate or refute the results of the testing and with assumed confidence in the accuracy of the FE solver, the focus of the investigation was predominantly concerned with the consistency of the model inputs with regard to the physical part. That is to say, the software results are totally dependent on the inputs and therefore must accurately reflect the part that was tested, in order to obtain comparable results. This new direction was brought to light by information obtained from the manufacturers of the metamaterial pad. Chiefly, the tolerances of the printing process and the material properties of test specimens produced from the same powder batch as the pad. Since the pad was specifically optimized to minimize the strain error between the expected and desired deformations, errors in those dimensions would undoubtedly impact the overall performance. Similarly, differences in material properties from one to the other directly impact the behavior of the beam and support elements while loaded. This approach would also be significantly easier to explore and offers the possibility to tweak the FE model based on those property and dimensional analyses. As a result of this narrowed direction of the investigation, we were able to determine three potentially influential factors that could explain a large portion of the difference between the two mechanical responses. They are as follows:

1. The assigned material properties in the model, which were provided by the manufacturer, may not reflect the material properties of the actual built pad.
2. The printing tolerances of the EBM process may result in dimensional variances between the model and the physical part since the parts may not be able to be printed at the required tolerances.

3. The loading and boundary conditions of the model may not be indicative of the experimental conditions experienced by the physical pad.

2.3.1. Material Properties Variances

One of the most intuitive reasons for the 3D printed backer pad not performing as predicted by the FE models is that the material properties assumed in the analysis are not consistent with the properties of the physical part. Additive manufacturing is an emerging technology, rapidly growing in demand and implementation across the high performance manufacturing community. However, literature suggests that accurate and repeatable material properties are not always a guaranteed result of the processes. In fact, a litany of factors exist that are known to greatly affect the predictability of material properties in these manufactured parts.

The most significant factors that can contribute to the inconsistency of material properties in AM parts are the qualitative and quantitative characteristics of the base powder used in production. In particular, the size and shape of the powder particles have shown to impart significant effects on the workability of the powder and the subsequent integrity of the final part [11][12]. The relative roundness, as well as smoothness or jaggedness, of particles can determine how the powder is distributed throughout each layer of the build. Jagged edges and non-uniform shapes can cause particles to catch on each other and clump. This can result in poor powder flowability and subsequent imperfections in final results [13]. On the other hand, uniformly shaped (round) and sized particles can have their own adverse effects if not properly controlled. Uniform particles stacked upon one other can leave significant voids, especially as particle size increases. These voids

effect the tap density of the powder, the final density and porosity of the parts, and thus the mechanical properties of the material [14]. In small part features especially, compromised material density can adversely affect performance. Even the storage of powders and the reuse of unbonded powder can impact the material quality.

Other factors that can negatively influence the material integrity of these manufactured parts stem from print process parameters, such as the part orientation during build and the path of the laser as it travels across the powder bed. Both of these can impact the homogeneity of material properties, creating anisotropic material characteristics in the x,y and z directions [15]. Powder layer thickness can also contribute to inclusions of unbonded material within the body of the part, causing localized inconsistencies and potential part failure [16].

While most of these aforementioned sources represent circumstances that are controllable in the manufacturing process, it is difficult to determine if they are root causes for the backer pad deviations with so few samples and no information about the printing parameters. There is, however, a relative range of expected properties that these printing process produce for each material. This provides a more predictable range of values, working under the assumption that the rest of the manufacturing parameters are in accordance with high quality prints. Therefore, for this particular investigation, the known range of the Ti-6Al-4V titanium alloy will be used to understand the influence caused by these more predictable fluctuations in property values. The results of this investigation will be presented with other sensitivity analysis results in Section 2.4.

2.3.2. Geometric Dimensional Variances

Similar to potential variances in expected material property values for the part, dimensional variances are a reasonable expectation for these additively manufactured parts. These variances could undoubtedly impact the overall behavior of these optimized parts, and can arise from a variety of sources. As with material property variances, printing process parameters are among the first sources to consider when investigating dimensional accuracy. For instance, powder layer thickness of the build platform has been shown to play an integral part in the final geometry of parts [16]. This thickness, combined with the intensity of the energy source, determines if a proper melt is achieved throughout the entire thickness of the layer. For areas along the perimeter of the cross section, this could result in imperfections of the edge geometry, as well as mass errors compared to the original part.

Another parameter, print direction, can also effect the achieved dimensions of a printed part [15][17]. In addition to effects on the homogeneity of material properties as discussed in Section 2.3.1, the orientation can determine the amount of complex curved or overhanging features. The number of small features and curved features has already shown to be a determining factor in the dimensional reliability of these parts [18], as has the presence of overhanging or unsupported features. These features, similar to truss structures, have been documented to have mass errors up to 30% smaller than anticipated final masses, resulting in significantly compromised parts [19]. When these two factors are potentially combined, the feasibly expectable error and associated mechanical behavior error drastically increase.

Additional factors can have adverse effects on the dimensional accuracy of these 3D printed parts, strengthening the case for an investigation into the effects that deviations from the optimized dimensions may have. Even under the assumption of consistent and idealized printing and powder parameters, documented errors with EBM printing, in particular cases, have shown to be 10-100 times larger than those associated with CNC machining of identical parts [20]. In the case of these metamaterials and other cellular structures, however, CNC methods are not viable manufacturing solutions and the benefits of the predicted mechanical behavior are too great. Therefore, the risk of larger errors is an unavoidable factor in the design process.

While these various factors have justified the examination of printing error effects of mechanical behavior, without additional parts or viable methods to examine and map the internals and topographies of these parts, printing parameters and powder characteristics will be assumed ideal. This leaves one standard source of error to be systematically tested, which is the known tolerance of the Arcam EBM printing machines and was provided to us by the pad manufacturer. This known tolerance is the tightest possible accuracy obtainable and provides the best case scenario of parameter ranges that the parts could assume. Provided by the pad manufacturers, the expected accuracy of EBM, at the current time and date of this thesis, is 0.1mm, which, when combined with a sensitivity analysis, could provide the range of feasible responses for the pad. This is discussed further in Section 2.4.

2.3.3. Accurate Modelling of Boundary Conditions

Being one of the three influential factors which could explain the obtained results, there was confidence that boundary condition modification would influence the model results, but the degree of the changes was unknown. When the experimental set-up is compared to the original conditions of the model, significant differences emerge in both the manner in which the load is transmitted and the constraints placed on the pad. Initially, the FE model utilized a uniform pressure across the top surface of the pad to apply the load. That coupled with a ‘fixed’ boundary condition on the bottom surface created the necessary conditions to compress and deform the pad. Additionally, sliding constraints were placed on the left and right edges, in an attempt to keep the deformation of the pad in the y-direction. All of these conditions can be seen in Figure 2.6 and further details of the model are available in [7]. While these initial applied constraints attempt to replicate the conditions of a pad fixed in the track system, it was clear that they did not accurately model the set-up for the experimental compression testing.

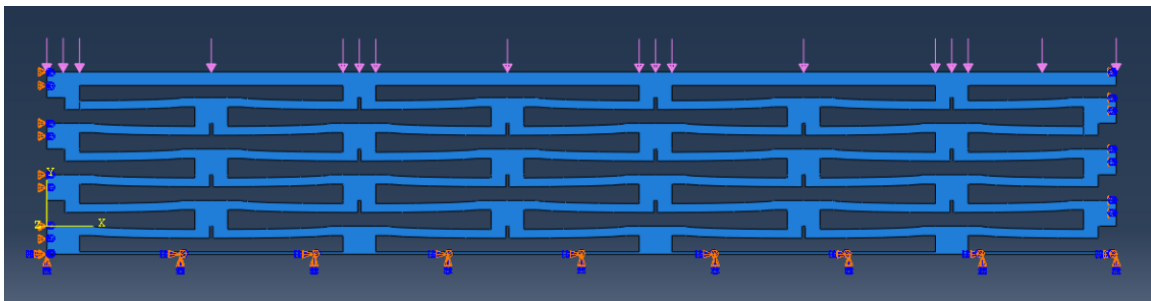


Figure 2.6 Original Boundary Conditions for the Backer Pad FE Model

Preliminary work was conducted to more accurately represent the experimental setup and associated boundary conditions. The experimental testing utilized two steel plates to sandwich and compress the pad, as shown in Figure 2.1. The original FE analysis,

however, was more simplistic, with a uniform pressure applied directly to the top surface of the pad and a combination of fixed and sliding boundary conditions constraining the system. To account for the differences, plates, and the corresponding contact they created, were modelled and added to the system. The addition of these plates introduced some new complexities to the system, such as the need for contact between the moving parts and a change from static loading to a dynamic ‘quasi-static’ loading, both of which required their share of troubleshooting. All these changes are documented in Figure 2.7. The top plate was used to transfer the pressure to the top surface of the pad and the bottom plate was used as the fixed body for the system, allowing the pad surfaces to become more unconstrained. This is important to note because as testing proceeded, upward deflections in the thin bottom layer sections of the pad were observed. While not overly impactful on the target behavior trying to be obtained, these small deflections were replicated once the compressive plates were added to the model and helped confirm that changes to the model environment were needed for more accurate performance.

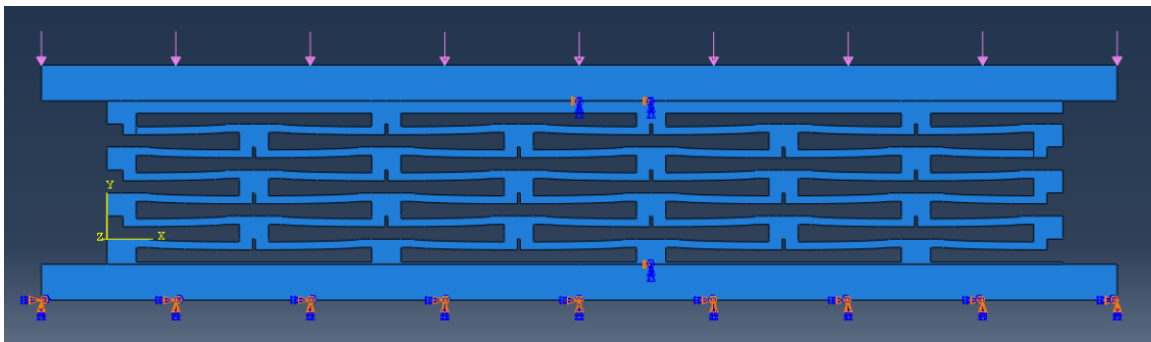


Figure 2.7 Modified Boundary Conditions for the Backer Pad FE Model

While initial results do show larger strains for the model, as shown in Figure 2.8, loss of nonlinearity in the deformations was unexpected and contrary to the corresponding

experimental results. Therefore, more research regarding the optimal ways to represent the contact between the moving parts of the experiment was warranted. Other factors had to also be identified, such as the coefficients of friction between the pad and plates and the most appropriate ways to assign boundary conditions and constraints to all the pieces.

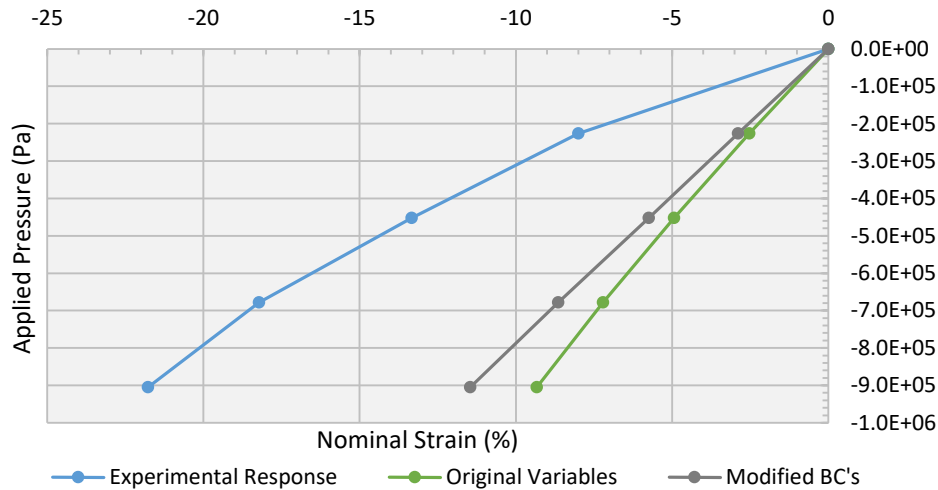


Figure 2.8 Changes in Mechanical Response due to Boundary Condition Modification

2.4. Sensitivity Analysis of Potential Material and Dimensional Inaccuracies

While cellular materials are highly desirable for their lightweight and unique mechanical characteristics, they present particular challenges when it comes to part manufacturing. The empty volume that is associated with cellular structures cannot be easily replicated using traditional manufacturing processes. The reliability of a structure designed using the UCS method is dependent on the level of precision with which it is manufactured. While the optimizer can produce ideal geometries, on the order of 10^{-6} m or smaller, the capabilities of AM technologies do not allow for such small tolerances. Thus, it is important to understand the impact of these inaccuracies through systematic exploration.

2.4.1. Design of Experiment Methodology

A sensitivity analysis can be organized as a matrix experiment, or a set of independent experiments with the same set of changeable parameters. The columns of the matrix represent each variable while the rows of the matrix represent the different experiment. Each individual cell is then populated with the desired value meant for that variable in that particular experiment. As the variable values are changed, the outputs of the experiments are impacted and the differences can be studied with respect to the changes from one experiment to the next. Orthogonal arrays are systematic matrices used to conduct a reduced set of experiments, but still allowing the effects of parameter changes to be efficiently and completely determined, at a much reduced computational cost when compared to fully exhaustive combinations of parameters and the significant number of experiments needed [21]. By changing the values of variables and observing the change in output, the level of influence that individual parameters have on a final solution can be obtained. By identifying this magnitude of influence, designers can more effectively prioritize which parameters require extra considerations and how to best mitigate the adverse effects of their manufacturing tolerances. Orthogonal arrays are typically used to conduct these design of experiments because of their relative ease in setup and the significantly decreased computational requirements. These arrays are organized in pre-determined sequences, based on the overall number of parameters that need to be examined. The array sequences also take into account the number of levels that are associated with the parameters. If variable significance, the amount of mechanical response change associated with a corresponding variable change, is expected to behave linearly

across the bounded interval, then a two-level array is all that is needed to explore the design space. However, if nonlinearity is expected across the initial interval, then using a three, or more, level array will best capture the varying degrees of influence with respect to the subintervals chosen [21].

For example, a $L_{12}(2^{11})$ array consists of 11 independent variables set at one of two levels, and is organized into 12 experiments. The first experiment uses all low values for the variables and the sequence of values for subsequent experiments is determined by a corresponding array table. Once the variables are adjusted for a particular experiment, the FE model can be run and the resulting mechanical behavior recorded. From the results, significance values can be obtained for every parameter, indicating the magnitude of impact any one variable holds on the overall behavior of the system, in relation to the other variables. The formula used to find these importance values is given in Table 2.1. The importance values provided insight into the amount of influence that any particular parameter has on the overall behavior of the metamaterial.

Table 2.1 Importance Value Equations and Definitions

Importance of Variable	$I = A_1 - A_2 $
Variable Definition	$A_1 = \frac{\sum \epsilon_{Low}}{n}$ $A_2 = \frac{\sum \epsilon_{High}}{n}$ $n = \frac{N}{2}$ <p><i>N = number of total experiments</i></p>

In addition to identifying independent significance, some of these arrays allow for the study of interactions between two or more variables to ascertain how changing multiple variables at the same time can compound or negate effects. These interactions hold great importance, as they help identify whether or not the variables with the lesser importance values can still have a dramatic impact on a system when coupled with other parameters. While the single parameter importance values only consider the difference in results after the change of one variable, the interactions, which are visualized in plots, look at the change in system responses for all permutations of level combinations between two variables. The magnitude of these interactions can vary, with a strong interaction indicating that two variables have a greater cumulative effect on the system, when simultaneously changed, than their individual significance values would suggest. This is visualized as two intersecting lines on the plot. As parallelism increases between the lines, interaction strength decreases [21]. This can indicate to designers whether homogeneous or heterogeneous level combinations produce discernable patterns of response. Therefore, a study of interactions should also be included with the base sensitivity analysis.

2.4.2. Sensitivity Analysis of Optimized Pad

The importance analysis was completed employing a $L_{16}(2^{15})$ orthogonal array, which is a design of experiments process that utilized the 14 dimensional variables and one material variable in a 16 experiment setup. This particular array is a two level array, meaning the variables are set at either a high or a low value, depending on a sequence predetermined by the corresponding orthogonal array table, shown in Table 2.2. These high and low values of the experiments were set at the feasible high and low parameter values,

give the error, and are represented by the red “1” and green “2” in the array table respectively. Once the variables were adjusted for the particular experiment, the FE model was run and the resulting strain values were recorded. From these strain values, significance values were obtained for every parameter, indicating which of the variables impose the most influence on pad behavior when changed. In the case of this analysis, the loads used were based on both the known static weight of the tank, distributed across the pads, and also the known limitations of testing apparatuses available at the time of any experimental testing. At operating weight, the M1 Abrams would transmit 22.5kN of load to any one of the 28 pads in contact with road wheels. This translates to roughly 1MPa of pressure across the pad surface. Table 2.3 shows the respective values for all the parameters at loads from 5kN to 20kN, as well as the average significance value across the entire load range.

Table 2.2 Orthogonal Array Table for $L_{16}(2^{15})$ Taguchi Array

	A	B	C	D	E	F	G	H	I	J	K	L	M	N	O
1	1	1	1	1	1	1	1	1	1	1	1	1	1	1	1
2	1	1	1	1	1	1	1	2	2	2	2	2	2	2	2
3	1	1	1	2	2	2	2	1	1	1	1	2	2	2	2
4	1	1	1	2	2	2	2	2	2	2	2	1	1	1	1
5	1	2	2	1	1	2	2	1	1	2	2	1	1	2	2
6	1	2	2	1	1	2	2	2	2	1	1	2	2	1	1
7	1	2	2	2	2	1	1	1	1	2	2	2	2	1	1
8	1	2	2	2	2	1	1	2	2	1	1	1	1	2	2
9	2	1	2	1	2	1	2	1	2	1	2	1	2	1	2
10	2	1	2	1	2	1	2	2	1	2	1	2	1	2	1
11	2	1	2	2	1	2	1	1	2	1	2	2	1	2	1
12	2	1	2	2	1	2	1	2	1	2	1	1	2	1	2
13	2	2	1	1	2	2	1	1	2	2	1	1	2	2	1
14	2	2	1	1	2	2	1	2	1	1	2	2	1	1	2
15	2	2	1	2	1	1	2	1	2	2	1	2	1	1	2
16	2	2	1	2	1	1	2	2	1	1	2	1	2	2	1

Table 2.3 Significance Values for Design Parameters of Backer Pad

Var	Load 1	Load 2	Load 3	Load 4	Average
t₄	0.59	1.09	1.49	1.81	1.25
E	0.36	1.02	1.42	1.77	1.14
t₃	0.41	0.78	1.10	1.38	0.92
t₂	0.48	0.83	1.07	1.22	0.90
G	0.32	0.59	0.81	0.98	0.67
H	0.22	0.40	0.53	0.64	0.45
r₂	0.15	0.32	0.50	0.67	0.41
f₂	0.11	0.19	0.25	0.47	0.26
f₄	0.11	0.18	0.21	0.24	0.18
f₃	0.07	0.14	0.20	0.25	0.17
W	0.06	0.13	0.20	0.27	0.17
f₁	0.07	0.13	0.16	0.18	0.14
BT	0.05	0.08	0.10	0.11	0.08
TT	0.03	0.04	0.05	0.05	0.04
r₁	0.03	0.04	0.03	0.02	0.03

The table indicates that the oval beam thickness (t_4) of the unit cell has the greatest impact on the behavior of the pad, with a value of 1.25, while the major radius of the oval beam (r_1) has the smallest impact on the system. What is not entirely understood by the table values, however, is the amount of fluctuation these values translate to, with respect to the expected response of the pad. To better visualize the influence of these single variable changes, Figure 2.9 shows the change in nominal strain of the pad with a 0.1mm change in t_4 and in r_1 . From the figure, it can be seen that the 1.25 significance value correlates to a roughly 11% change in mechanical behavior in the test load range. As loads increase, the percent change decreases, but still shows significant variation from the target. The r_1 value, on the other hand, shows an identical deformation response to the expected behavior.

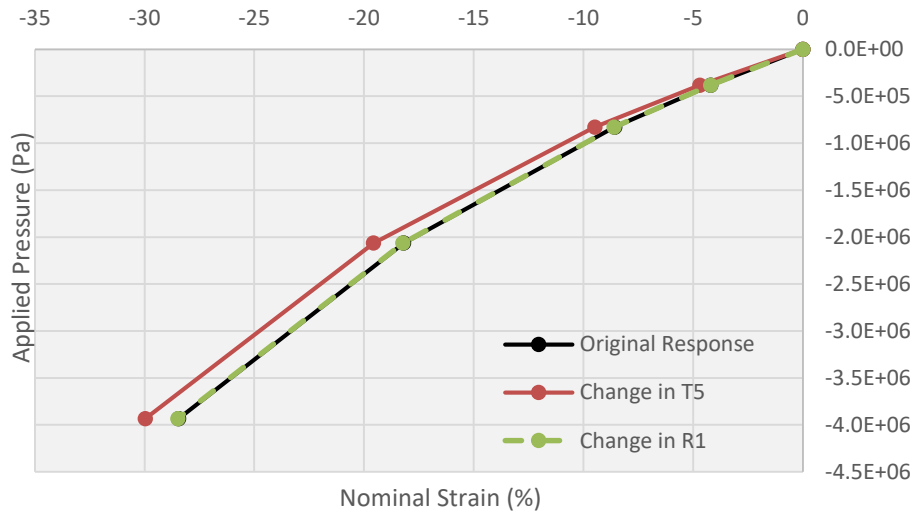


Figure 2.9 Effects of Most and Least Significant Parameters on Pad Behavior

2.4.3. Interaction Plots

In addition to the individual significance of the design parameters, we investigated whether or not the variables with the lesser importance values can still have a dramatic impact on the part when coupled with other parameters [21]. To do this, a study of interactions was also completed. As described in Section 3, these interactions are visualized using plots, such as the one pictured in Figure 2.10. This particular plot shows the interaction between OB thickness (t_4) and unit cell half width (W). To obtain the lines, first the results of any experiments which feature the same high-low combination for any two variables, A and B , are averaged. In the case of a 16 experiment array, there are four experiments that feature A_1B_1 , four that feature A_1B_2 , four that feature A_2B_1 , and four that feature A_2B_2 . This provides averages for the high-high, low-low, and two mixed pairs of experiments. Plotting the averages of both levels of A with B_1 and then B_2 provides the two interaction lines, which can be seen in Figure 2.10. The parallelism of the resulting lines

indicates the strength of interaction between the two variables. Intersecting lines mean a strong interaction exists, while parallel lines indicate no interaction is present. In the case of Figure 2.10, the results suggest that when W (A) and t_4 (B) are altered in conjunction, there is a compounded effect on the pad with respect to the independent significance values of the two dimensions. On the other hand, plots with weaker interactions behave in more accordance with the respective significance values. In the figure, B_1 represents the line between the averages when B is low, while B_2 represents the line between the averages when B is high.

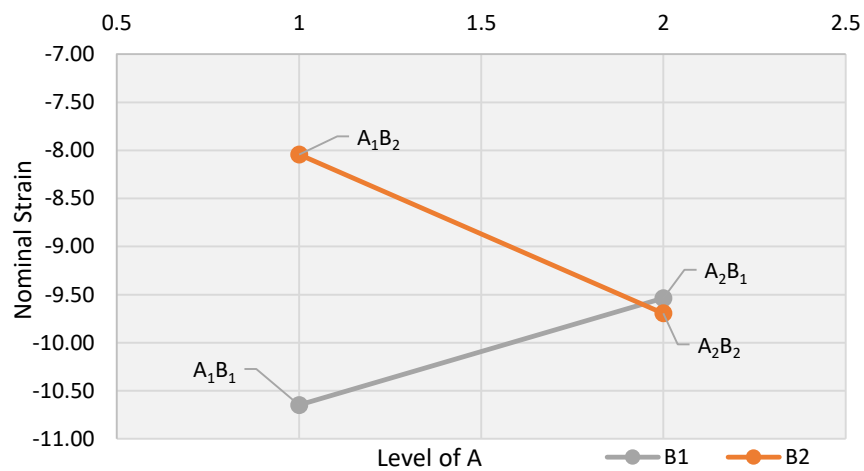


Figure 2.10 Unit Cell W and CB Thickness Interaction Plot

By constructing additional plots, and observing similar interactions between the half width of the cell and thicknesses of the EFGs and ESGs, it could be determined that a significant pattern existed between these two types of parameters. This finding encouraged interaction plots for other variable combinations to be constructed and observed. Using the thicknesses, in conjunction with variables like cell height and the major radius of the oval beam, continued the pattern of results. It was subsequently discovered that these

compounded interactions were caused by combinations of increases and decreases of variables that provided larger deviations than increasing all or decreasing all the variables. For example, increasing W while decreasing t_2 produced a softer overall pad, as did similar mixed changes with variables like H and other thicknesses. This conclusion, while not entirely obvious, does make sense. Increasing the width of the unit cell increases the span of the cantilever beam and the moment about the beam tip. Decreasing the beam thickness can result in increases in deflections experienced by the beam under an equivalent applied load. When combined, this increase in L and decrease in t result could result in a disproportional increase in deflection, according to elemental beam theory, explaining the compounded interaction of these two, and similar combinations of, variables.

Ultimately, the tolerance investigation was meant to determine how much of the mechanical response deviation between the FE simulation and experimental results could be plausibly but reasonably accounted for through manufacturing error. Since the experimental testing produced softer than expected results, the softest possible model pad is needed for comparison. By understanding the variable interactions within the pad, the ideal combination needed to for this particular response can be selected. By increasing H , W , and r_1 and decreasing the others, the greatest pad deformations are obtained. This response can be seen in Figure 2.11, where a 25% increase in strain is observed as the softest response. Similarly, a 25% decrease in strain is observed by flipping the tolerances to the other end of the range. When compared to the experimental deformation behavior, however, these changes account for just over a third of the total difference. This identifies a large range of feasible behavior trends for these parts and provides an interesting potential

challenge for designers and the implementation of these analyses. Trying to minimize the error between desired and potential extreme responses could result in more desirable cell configurations, resilient to manufacturing limitations.

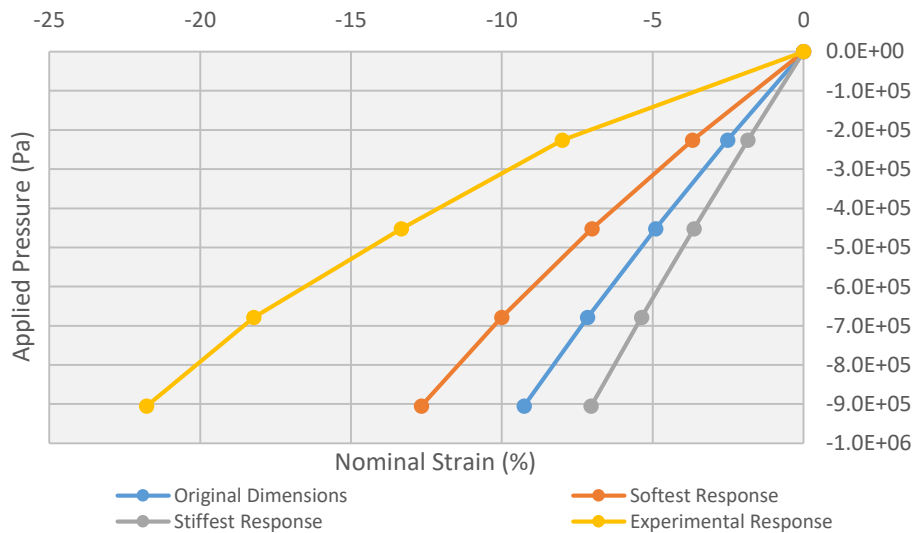


Figure 2.11 Potential Effects of Printing Tolerances on Backer Pad Performance

2.4.4. Significance of Material Property Variances

From the results of the sensitivity analysis, and Table 2.3, it is revealed that the material property changes rank third in overall significance with respect to mechanical behavior impact. Unlike the significance values of the dimensional parameters, which were judged on 0.1mm changes, the material property significance was determined by a 12GPa change in Young’s modulus (E). However, both of these variable ranges represent the maximum deviation that can be expected from the printing process and, therefore, make it difficult to compare them against each other. Decoupling Young’s modulus from the other variables will allow for the independent examination of its singular effect of the system, confirming or refuting the first of the potential explanations outlined in Section 2.3.

Thus, Figure 2.12 shows the effects of setting the Young's modulus to both the upper and lower extremes of the expected powder range. From the chart, one can see that significant deviations in mechanical behavior are experienced with these modulus changes, as expected. Within the current operating ranges of the backer pad (up to ≈ 1 MPa), the changes in E produce a near 10% change in the displacements incurred by the pad. While it does not come close to accounting for all of the difference, this result is particularly significant given the total change in E is only 11-12GPa and could potentially explain a portion of the disparity between the numerical and experimental results. It is also important to note that the change in material property values does not visibly impact the nonlinearity of the system, only strengthening its argument as a viable piece of the overall explanation since the experimental behavior maintains the desired nonlinear characteristics.

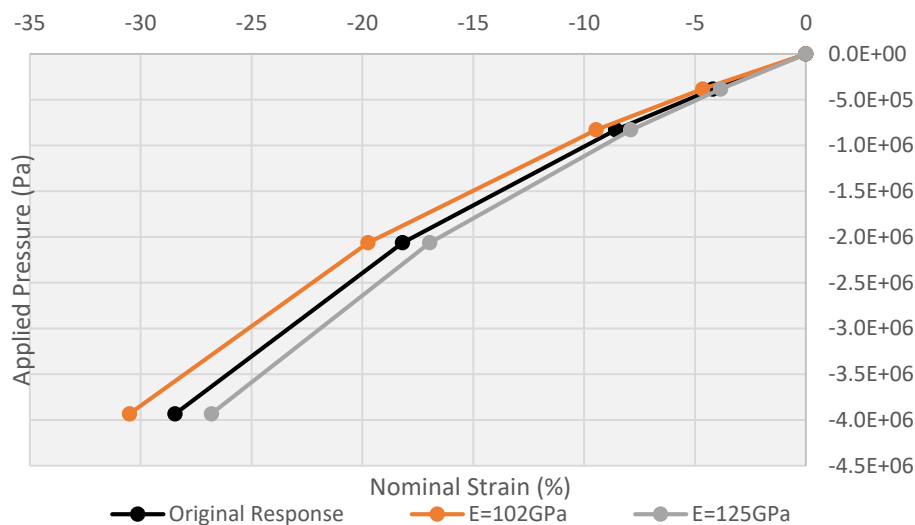


Figure 2.12 Effects of Material Property Changes of Backer Pad Behavior

2.5. Results and Discussion

Ultimately, the goal of this analysis was to address the third major research question by validating the three potential sources for mechanical behavior discrepancy initially identified. By obtaining the range of mechanical performance, given the acceptable variations in design parameters, the independent influences of these potential sources were identified. However, to capture the most complete expectation of the backer pad's mechanical behavior given the least ideal manufacturing quality, the independent sources needed to be combined. This would provide a worst case scenario, of sorts, both above and below the expected behavior of the pad. Given the limited investigation into the suspected boundary condition inaccuracies, the puzzling results produced by their manipulation, and the need for more investigation to be done, the final result will only combine the effects of material property and dimensional parameter variations.

As a result, Figure 2.13 shows the combined effects of both potential sources of error, and provides a look at the limits of stiffness and softness that could reasonably be expected from the UC design, under given manufacturing parameters. The corresponding design variables can be found in Table 2.4. Though the pad was optimized with the intention of behaving in accordance to the rubber backer pad, the physical specimen may not behave as such. The largest deviation possible under the allowable error provides a direct view of the bounds and a map for further optimization of the metamaterial. Additionally, the chart shows that when the material and dimensional effects are combined, roughly 50% of the total discrepancy could be accounted for.

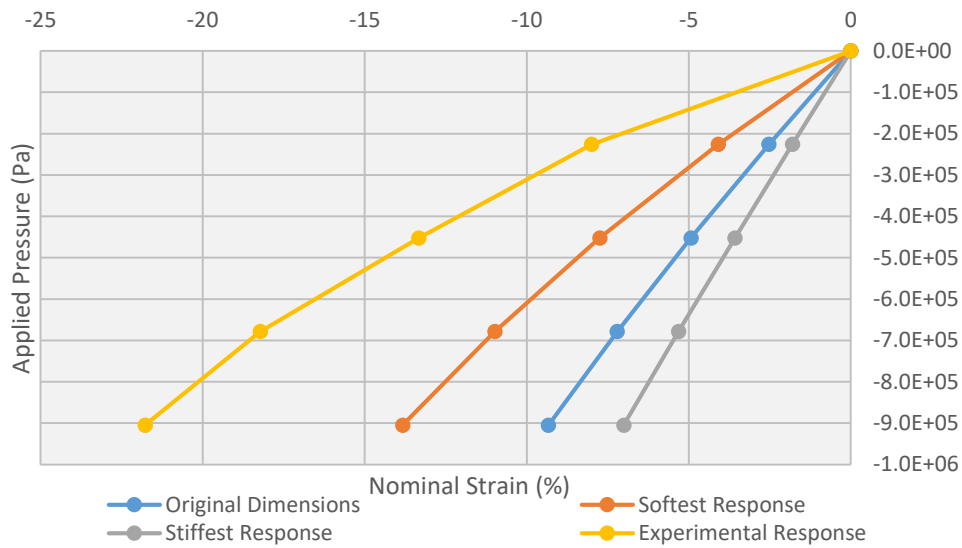


Figure 2.13 Upper and Lower Bounds of Deformation Behavior for Metamaterial Pad

Table 2.4 Parameter Values for High and Low Responses

Variable	Original	Stiffest	Softest
W	20.5mm	20.4mm	20.6mm
H	3.20mm	3.10mm	3.30mm
t ₂	1.15mm	1.25mm	1.05mm
t ₄	1.58mm	1.68mm	1.48mm
t ₅	1.04mm	1.14mm	0.94mm
g	0.39mm	0.49mm	0.29mm
r ₁	11.60mm	11.50mm	11.70mm
r ₂	0.45mm	0.55mm	0.35mm
BT	0.30mm	0.40mm	0.20mm
TT	1.70mm	1.80mm	1.60mm
E	114 GPa	125 GPa	102 GPa
Fillet 1	1.00mm	1.10mm	0.90mm
Fillet 2	0.75mm	0.85mm	0.65mm
Fillet 3	0.30mm	0.40mm	0.20mm
Fillet 4	0.55mm	0.65mm	0.45mm

2.6. Proposed Implementation of Sensitivity Analyses in MUCS Method

Implementing these analyses in the evaluation of final material designs could prove essential in predicting the worst case scenarios for an AM manufactured part.

Running the experiments will generate the significance values of the particular unit cell as well as a glimpse at what the softest and stiffest potential mechanical responses could look like. This information would provide insight into the feasibility of consistent performance across large scale production, as well as encourage the further development of unit cell designs that resist the influence of known printing deficiencies.

CHAPTER 3. BEHAVIORAL INVESTIGATION AND OPTIMIZATION OF CIRCULAR META-MATERIAL FOR TANK ROAD WHEEL

3.1. Meta-material Design Requirements

As discussed in Chapter 3, elastomer bodies are utilized in several locations throughout the tank track system. Upon gathering a more complete understanding of the initial metamaterial backer pad design, the expansion of the method implantation could begin to target other vulnerable elastomer materials and address the need for a full system investigation. But, to properly answer RQ2, regarding a meta-material system design, a new research question must first be explored. RQ2.1 highlights the need to, first and foremost, design and optimize a circular meta-material for implementation on the road wheel, providing greater feasibility for the eventual system approach. This new question is:

RQ2.1. Using the Modified UCS method, can a meta-material circular layer for the wheel be designed and optimized to match the nonlinear responses of the original rubber components?

To obtain the appropriate design, the Modified UCS method must be employed with some slight adjustments to accommodate the circular nature of the road wheel. This will not only alter the approach to the beam element selection for the UC, but will also require modifications to design variables to ease manipulation in the optimization efforts that follow.

3.1.1. Unit Cell Selection for Polar Mapping

An immediate challenge that was faced in the design process for a replacement road wheel material was the overall shape that the material had to assume. The initial meta-material pad was designed in a Cartesian frame of reference, where the straight and curved EFGs could be easily represented and modelled. The road wheel contour, however, requires a meta-material designed in a polar frame of reference, with the x and y directions being converted to the radial and circumferential directions. For straight beams, this mapping into the polar coordinate system is straight forward, with the new elements following a circular path. However, the use of initially curved elements can pose more of a challenge, since the mapped material inherits its own curve around the wheel. For this reason, the initial linear configurations considered for this new meta-material used only straight beam elements, mapped to fit the rim of the wheel.

Keeping with the MUCS methodology, a model of a rubber lined wheel, compressed against a rigid surface, was evaluated at four loads to gather design targets for eventual optimization, shown in Figure 3.1. This model, while not immediately reflective of the entire track system, contained fewer mesh elements and deforming parts and required less computational commitment to solve. Like in the original case study, the rubber material was defined using a second-order Ogden model. Given the deformation trend data gathered in the original case study [7], which is shown in Figure 3.2, the ‘canti-duo’ design showed great promise as a UC configuration for this ‘meta-band’ to match the desired behavior. The original representation of the ‘canti-duo’ design, shown in Figure 3.3, exhibited tailorable nonlinear characteristics under loading and proved, during the original

pad case study [7], to be a feasible optimization candidate. The simplicity of the UC was also an influential characteristic for its consideration as the initial selection, providing ease of modeling and implementation of optimization considerations.

The unit cell utilizes two cantilever beams (CBs) fixed to the cell's corresponding ESGs and separated by a distance, $2g$. When tessellated into a multi-layer, continuous material, the half-cell offset between subsequent layers provides a path through the ESGs for force transmission to the tips of the CBs.

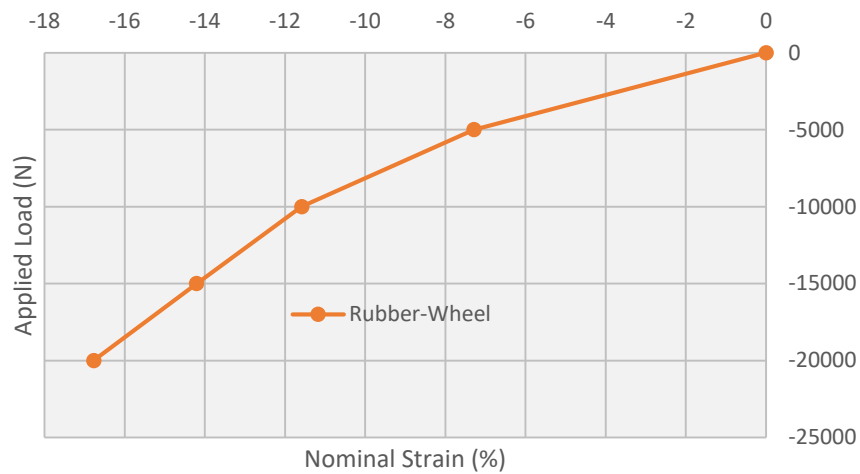


Figure 3.1 Target Mechanical Behavior for Initial Meta-band Optimization

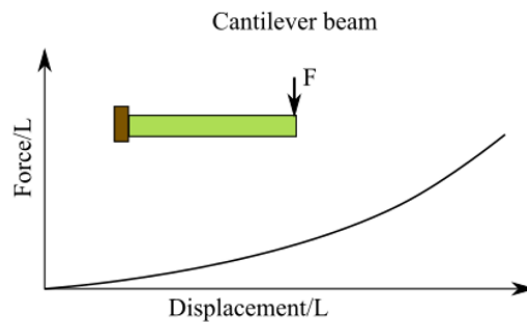


Figure 3.2 General Deformation Behavior of Canti-Duo UC Design

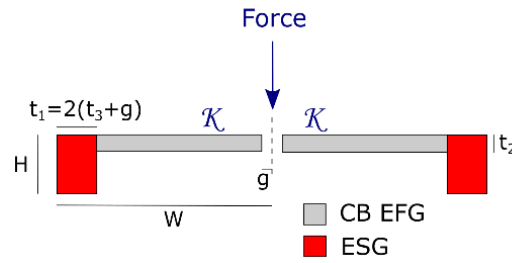


Figure 3.3 Canti-Duo Unit Cell Design

3.1.2. Design Variable Modifications

By using the ‘canti-duo’ unit cell design for the circular profile of the road wheel, certain considerations and modifications need to be made to ensure feasibility of tessellation. The largest change to be made to the UC design is converting all of the linear distances into angular measurements. In order to maintain the 50% offset from layer to layer and to ensure that each layer of the material contains the same number of cells, like the original pad, the UC half width (W) is converted to an angle. Since the material must be a closed loop of cells around the perimeter of the wheel, the number of valid values for W are limited to those that would produce an integer, n , number of complete cells per layer. That is to say, if W is equal to 3 degrees, each unit cell would be 6 degrees in width and the material would contain 60 cells per layer. Contrarily, if W is to equal 7 degrees, the UC would be 14 degrees wide and the resulting material would contain 25 full cells and an incomplete 26th cell. Other dimensions that are converted to angular values are the gap (θ_2) and ESG thicknesses (θ_3). These changes serve a two purposes. First, using angular values makes the modeling process for the material significantly easier. Second, the use of angular values provides consistency in the ratio of cell width and the relative ESG and gap

thickness. As the arc length of each layer increases, so too will the corresponding thicknesses of that layers gap and ESGs.

The remaining variables, such as height and cantilever beam thickness remain unchanged, since their values are oriented in the radial direction and require no angular consideration. The updated cell configuration is seen in Figure 3.4.

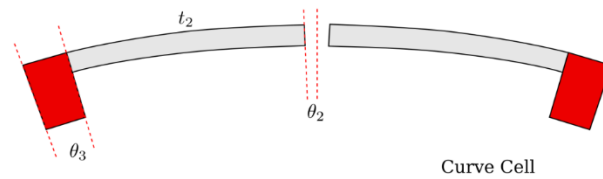


Figure 3.4 Modified Canti-Duo UC for Meta-Band

3.1.3. Meta-band Design for Multi-objective Optimization

For the purposes of the ‘meta-band’ design, a three variable UC, like the one in Figure 3.4, is used. The three changeable design variables are the cantilever beam thickness (t_2), the ESG angle (θ_3) and the gap angle (θ_2). The height (H) of the unit cell is set to a value that would ensure the overall height of the metamaterial is in accordance with the total rubber layer it is replacing. Additionally, some basic calculations must be done to determine a value for W that would not only provide a tessellation with no partial cells, but that is also consistent with the width of the original metamaterial pad’s cells. Since the ultimate goal is to study the interaction of both optimized materials, the cells are initially set to be of the same magnitude in size.

With the design variables and fixed values determined, the UC design is tessellated and added to the road wheel, as shown in Figure 3.5. In the figure, the cells appear inverted. This is because the interaction between the road wheel and any other

material occurs at the relative ‘bottom’ of the wheel, similar to a car tire on the road. Additionally, to save computational resources, only a 64-degree section of the meta-band and wheel is modeled as the representation of the road wheel. This provides a sufficient part size to capture the deformed section of the metamaterial, while keeping the number of elements in the model to a minimum. Additionally, internal deformation of the wheel band model dissipates to zero within 30 degrees of contact in both directions. Therefore, 64 degrees is adequate to ensure that all important mechanical behavior is observed and uninfluenced by potential edge effects of the material. A list of the dimensional variables for the design is provided in Table 3.1.

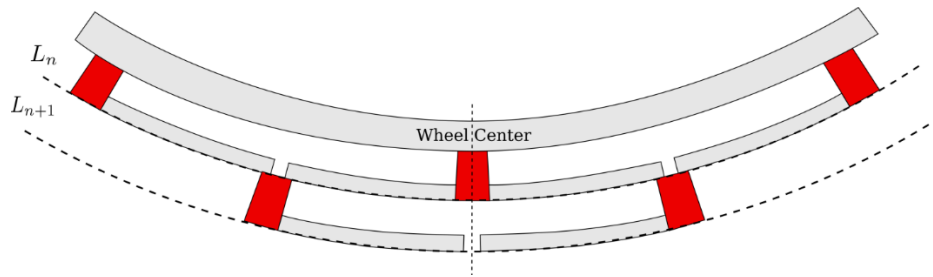


Figure 3.5 Tessellated Canti-Duo UC for Meta-Band

Since the requirements of the meta-band are comparable to that of the original meta-material pad in terms of deformation and stresses incurred, the expectations for the material properties are unchanged from the original case study. As described in previous work, a material that exhibits a high ratio of yield stress to Young’s modulus ($\sigma_y:E$) is needed for the pad due to the large deformations that would be experienced [7]. This would prevent yielding of the material while ensuring the proper stiffness. Therefore, the same type of titanium alloy used for the meta-material pad is chosen for the meta-band, with a Young’s modulus determined by the experimental data of backer pad manufacturers. The

density was not provided in the testing results and, thus, was based off the material selection of the backer pad [7]. The material properties for the meta-band are listed in Table 3.1 as well.

Table 3.1 Initial Meta-band Design Variables & Material Properties

Dimensional Variables		Material Values	
UC Height	H	Young's Modulus	114 GPa
UC Half Width	θ_1	Poisson's Ratio	0.32
CB Thickness	T ₂	Density	4820 kg/m ³
Gap	θ_2		
ESG Thickness	θ_3		

3.2. Initial Meta-Band Optimization

3.2.1. Abaqus Parameterization & Workflow

With the updated version of the modeFRONTIER (mF) software package came necessary updates to the original optimization process. In previous work, the optimization procedure was dependent on python scripts that mapped out the FE model generation, job creation, and eventual execution. The results were then extracted and externally processed before being analyzed by the optimizer. While there are advantages to the scripting based approach, accounting for the increased model complexity of the meta-band and eventual total system proved to be more involved than using the FE software's own GUI to create and assign the necessary material properties, meshes, outputs, etc. The new mF package includes direct tie-ins to the CAE software of choice, ABAQUS 6.14, allowing models to be directly imported into the optimizer, variable and output connections to be simplified, and errors to be troubleshot more effectively. The only scripting comes from a python file dictating the selection of the appropriate CAE file, a generic change in design variables for

the scheduler to mimic, regenerating and remeshing the part to account for parametric changes, and the changes in applied load to create the four separate jobs. While sounding complicated, all of these steps are captured in an automatically generated python file while working in the GUI.

The inclusion of the CAE specific tie-in presents the opportunity for all models to be preemptively parameterized within the software itself, one of the original advantages of the scripting method. This allows all dimensions to be defined in terms of a variable or variables and to be efficiently changed according to the design scheduler. Also, by simply changing the status of a particular variable to active/constant, the designers can control which of the design variables are available to the scheduler for manipulation. In the case of the meta-band optimization, a couple of the original UC design variables are deactivated. The height of the UC is fixed, due to the newly incorporated contact between the road wheel and the rigid surface. By altering the overall height of the metamaterial, that relative point of contact would be altered with each design iteration, leaving the model susceptible to failure. Such errors add time to the optimization process and can lead the optimizer to converge on a local optimum. The UC half width is also fixed for the reasons described in previous sections.

The last major modification made to the optimization procedure is changing the number of designs that could be run concurrently within any given generation. Using the Palmetto supercomputer to increase the number of processors available, all 10 designs of each algorithm generation could be run at once, cutting the expected time of completion down from 10 days to about one day. This is possible because the NSGA-II algorithm uses

the results of the initial 10 DOE points, determined using a Uniform Latin Hypercube, to generate the next 10 designs, the results of which are independent of each other. The pattern continues in this manner, effectively exploring the design space until the number of desired generations has been reached or the procedure is stopped.

3.2.2. Results and Discussion

After several hundred design iterations were run, the optimization procedure was halted, with relative convergence achieved. Unfortunately, the convergence that was obtained produced strain error values outside of the desired error constraint. The response of the design that produced the best strain error value can be seen in Figure 3.6, which is plotted against the target response and the response of the initial dimensions chosen for the meta-band. While the figure emphasizes the large discrepancy between the target and obtained result, it also shows the high level of behavior manipulation that is present in the meta-band design.

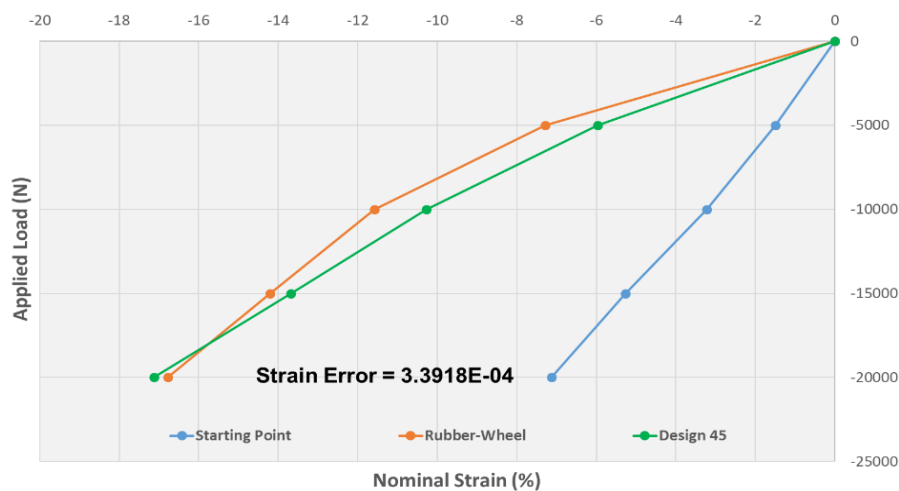


Figure 3.6 Results of Initial Canti-Duo Meta-band Optimization

Another take away from the results of the optimization is that, while nonlinear behavior is achievable in the meta-band, the level of stiffening which is experienced by the material is still less than ideal compared to the stiffening of the elastomer material. This sparked the formulation of an additional research question regarding the implantation of methods, by which designers can assume greater control of the stiffening or softening characteristics of these meta-materials.

3.3. Introduction of Size Factors for Increased Nonlinearity

Traditionally, UC based materials are designed using topology or shape optimization, where a single unit cell is optimized to meet targeted mechanical behavior. The resultant cell is then tessellated in the x and y directions to generate a complete material that exhibits the desired global properties. While this uniformity across the entire material has its's design benefits and ease of scalability, the materials are capped in the achievable level of complexity. The unit cell of the first row first column, for example, is the exact same as any other unit cell in the material, regardless of row or column. By adding additional variability in these tessellation directions, the range of expected responses could be potentially expanded. Because of the suboptimal nonlinear behavior exhibited by the 'meta-band' in the initial optimization, a new research question was formed in an effort to investigate a method to add even more control on the degree of nonlinearity in the meta-material. Utilizing the lack of variability in cell dimensions from layer to layer, the introduction of unique layer multipliers, dubbed 'size factors', was suggested to provide an extra level of complexity to the materials and adding up to an additional n number of

variables to the model, depending on number, n , of cell layers. Specifically, the resulting research question is:

RQ2.2. Can the introduction of ‘size factors’ impose greater variability on the degree of nonlinear behavior exhibited by Modified Unit Cell Synthesis method designed meta-materials?

To answer this new question, some changes have to be made to the ‘meta-band’ model, while modifications have to be made to the optimization workflow to handle the newly introduced variables. This is touched upon in subsequent sections. The primary concern, however, is developing the manner in which these factors would be eligible for application to any metamaterial designed using the modified UCS methodology.

3.3.1. Application of Size Factors

While the inclusion of these size factors does not change the overall design of the unit cell, it does change the manner in which the metamaterials have to be modeled. By modeling a half-cell thick section of the entire height of the pad, each size factor can be independently considered in its corresponding layer. From there, the sliver of cell layers can be mirrored until full tessellation is complete in the x or circumferential directions, depending on the overall orientation of the material. Figure 3.7 shows how the size factors are applied to a canti-duo UC design, for the meta-band or other meta-material, while Equations 3.1 and 3.2 show the how to determine the thicknesses of any particular cell layer’s EFGs and ESGs.

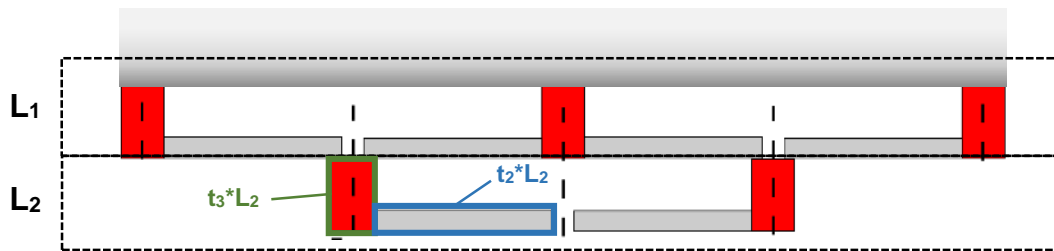


Figure 3.7 Size Factors Applied to a Canti-Duo UC

$$CB \text{ thickness for Layer } n = t_2 \times L_n \dots\dots\dots (3.1)$$

$$ESG \text{ thickness for Layer } n = t_3 \times L_n \dots\dots\dots (3.2)$$

One advantage of modeling the material in this particular manner is that the relative equations for determining the dimensional values of cell layers can be altered to include more than just the beam elements. If designers choose to manipulate the height of the cell as well, a quick change in parentheses could accomplish this. In the case of the ‘meta-band’, altering the height of the cells would result in a change of the overall material height, thus altering the point of contact in the multi-bodied system. This can result in errors within the FE solver and additional time to trouble shoot. Unless the obtained results dictate a further exploration of other variables to include in the optimization, the height remains fixed.

3.3.2. Initial Assumption

When initially discussing the addition of these cell dimensions multipliers, speculations were made in regard to the values that they would assume and their relative organization from layer to layer. In the case of the initial meta-band optimization, the nonlinearity obtained was not large enough compared to the target. The amount of deformation at the smaller loads needed to be larger. In tandem with those larger

deformations, the level of stiffening as loads increased needed to be greater. It was also determined that since the arc lengths of the outer most cells are larger than those closer to the center of the wheel, they would experience larger initial deformations if their beam members were thinner. When compared to interior cells of the same beam thickness, the larger arc length would produce a larger moment about the fixed point of the CB, thus producing larger displacements. This can be substantiated using classic beam theory for deflections of a point loaded cantilever beam, shown in equation 3.3.

$$\sigma_x = \frac{FL^3}{3EI} \dots\dots\dots(3.3)$$

Here, F is the force applied at the tip of the beam, I is the moment of inertia, E is the Young's modulus, L is the length of the beam, and σ_x is the deflection. One can see that the deflection, σ_x , is heavily dependent on the length of the beam, with a doubling in beam length resulting in an eight-fold increase in deflections. This equation is overly simplistic for the nature of the true deflections experienced by these beam elements, but speaks more to the general thought process used to predict the eventual organization of these size factors.

As a result of this recognition, it was hypothesized that the logical order these size factors would assume in an optimal design would be a graded based organization, such that:

$$L_1 > L_2 > L_3 > \dots > L_n, \dots\dots\dots(3.4)$$

where L_1 is the inner most layer of the 'meta-band', and L_n is the outer most layer. By using this graded assumption to constrain the optimizer's search to this particular design space,

it was expected that more efficient convergence could be obtained. A visualization of this proposed graded organization can be seen in Figure 3.8.

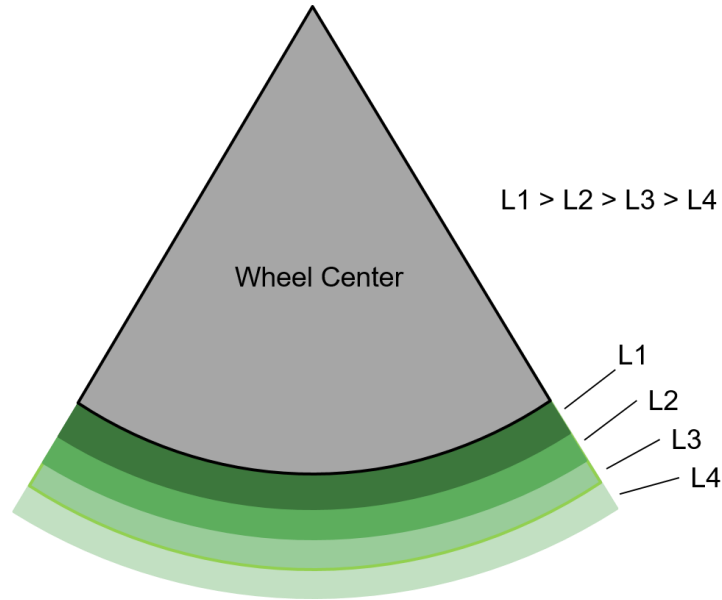


Figure 3.8 Representation of Gradient Based Size Factor Organization

3.4. Re-optimization of Meta-band with Size Factors

While it was initially assumed that the ideal organization of size factors would follow a graded pattern, two models were created for the subsequent optimization procedure. The first of the two models utilized the organized approach to the size factor application, while the second model used an unorganized approach, allowing the seven size factors to assume any value, in any order the optimizer determined fit. As for the optimization procedure itself, the project file from the original ‘meta-band’ optimization could be repurposed with minor modifications since the methodology remains unchanged.

3.4.1. Adjusted Parameterization and Optimizer Workflow

To implement the size factors into the ‘meta-band’ model, and subsequent metamaterial FE models, additional parameters were needed. Since the new variables were simply multipliers associated with each level, no additional features needed to be generated for the part. Instead, the correct assignment of factors and manipulation of the part within the solver had to be ensured. The base geometries of the cell elements were left intact, such that every cell in the material consisted of the same base variables. Size factors were then added in the ‘parameter manager’ of ABAQUS, each assigned to a layer of cells. These factors were then applied to the base geometries to generate independent values for each layer of cells. This progression of feature manipulation would allow the designer to activate as many or as few size factors as necessary. If factors were not needed, simply setting the value to 1.0 would ensure that the particular layer’s geometries would be that of the optimized base values.

Additionally, patterns of values could be set, such as one factor for every n cells etc, by adding simple constraints to the workflow. In the case of our initial assumption, a series of constraints were established such that the size factors would assume values less than the factor that comes before it. The general constraint, in terms of L_n and L_{n-1} is shown below in Eq. 3.5.

$$L_{n-1} - L_n > 0 \dots\dots\dots (3.5)$$

These constraints would establish the graded pattern of values and, in theory, help guide the optimizer towards what was believed to be the final organization. This is done to

help the efficiency of convergence for the optimization and reduce the time and resources required to obtain it.

3.4.2. Optimization Results and Discussion

After the 10 initial DOE points were evaluated for the organized size factor model, the optimizer was set to run an additional 490 design points determined by the genetic algorithm. However, upon reaching design 350, it was determined that the optimizer had converged on a Pareto front of relative optimal designs and greater convergence was unlikely. A chart of the design evaluations with respect to the obtained design objectives is shown in Figure 3.9. Unfortunately, none of these 350 evaluated designs met both the strain error and maximum stress set forth in the design objectives and, therefore, returned a mark of ‘real and unfeasible’ in the final design breakdown. This is shown by the chart in Figure 3.9.

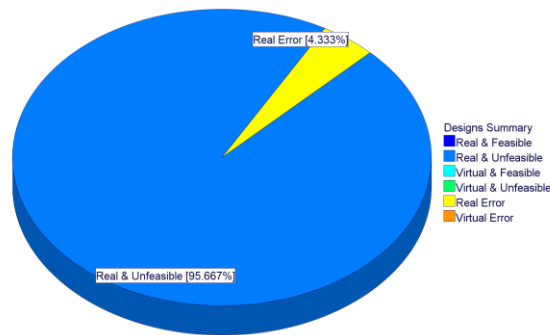


Figure 3.9 Meta-Band Optimization w/ Unorganized SF Design Summary Chart

While none of the designs met the desired strain error, the most optimal designs showed improvement for the uniform meta-band performance. In Figure 3.10, one can see the target load-strain relationship compared to best result from both the original

optimization and the organized size factor optimization. While the results are positive, room for improvement still exists and more investigation was required to obtain it.

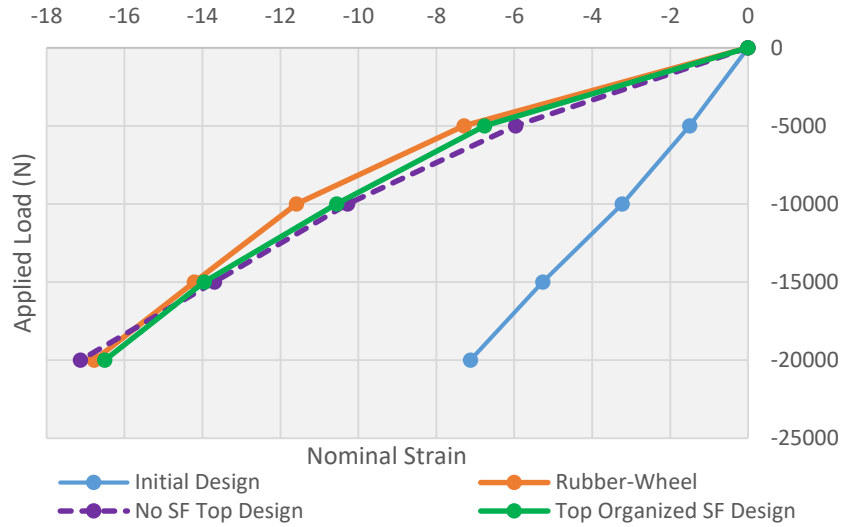


Figure 3.10 Mechanical Response of Meta-Band w/ Unorganized SF & No SF

Upon obtaining the results for the organized size factor model, the unorganized model was run, to determine if a greater agreement with the target deformations was achievable. Similar to the organized factor approach, the initial 10 DOE points were evaluated, with the intent of generating 490 additional design points. After an additional 300 design evaluations, the optimizer achieved sustained convergence for both of the design objectives. Remarkably, and contrary to the organized factor model, more than 30% of the evaluated designs met both of the design constraints and were marked as ‘real and feasible’, which can be seen in Figure 3.11. If the optimizer had been allowed to continue towards its 500 design evaluation goal, this number would have undoubtedly been higher, however, to conserve resources and continue our investigation into the meta-material bodies, the process was halted. The 4% ‘real error’ slice on the pie chart represents the set

of designs that either produced faulty geometries or resulted in aborted jobs in the FE solver. The nature of the genetic algorithm, however, can overcome these failures and continue to push the solutions towards the optimum by using its mutations and crossovers to effectively explore large swaths of the design space. This allows for designs with slight variations from their error producing counterparts to be evaluated and reveal the path to convergence. Additionally, Figure 3.12 shows the total design space, clearly marking the point where the obtained results begin to meet the design criteria. The tradeoff between strain error and maximum stress is also clearly visible, as the stress tends to spike with decreasing error. The one outlier, however, is the optimal design, exhibiting the lowest value for both objectives within the feasible range.

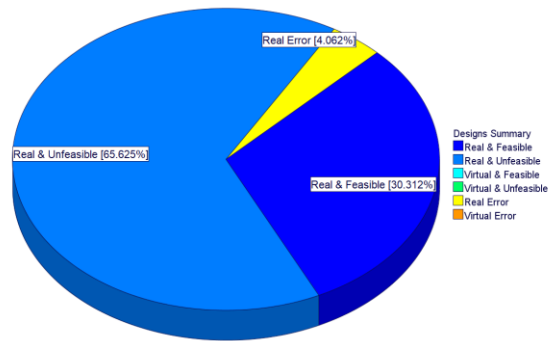


Figure 3.11 Meta-Band w. Unorganized SF Optimization Design Summary Chart

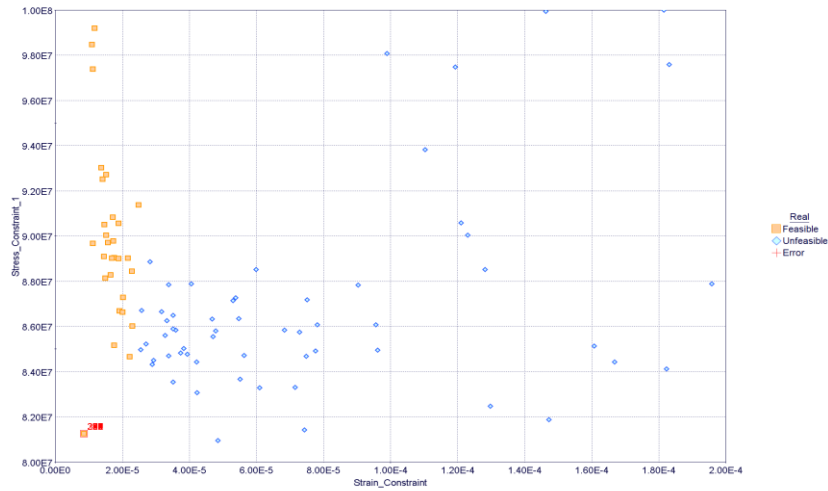


Figure 3.12 Meta-Band w/ Organized SF Optimization Design Chart

This outlier could be a result of the large step size set for these design parameters within the optimization scheduler itself. Since manufacturing limitations keep the viable decimal values of these variables to the order of 0.1mm, using design parameter values with four or more decimal places becomes unnecessary. Such small changes not only significantly increase the size of the design space, but also produce changes in the variable values that cannot be reciprocated in final manufacturing. This larger step size helps to ensure manufacturing differences between potential design options, however, it can leave larger gaps between explored designs. Additionally, initial population size has been shown to effect the speed and final distribution of NSGA-II based optimizations [22][23]. Smaller population sizes are best suited for faster convergence in potential computationally expensive problems, as less time is spent randomly searching in the early generations. However, faster convergence sacrifices comprehensive exploration. In some problems, small population sizes, relative to the problem, have shown to return unconvincing

diversity in the final design space [23]. This highlights an additional tradeoff that could require consideration in the future.

From the strain error values accompanying the list of Pareto designs, several optimal designs could be found, all of which show a significantly increased level of consistency with the target responses when compared to the best design of the organized size factor optimization. Figure 3.13 shows the mechanical behavior of the top design layered on top of the target response. The two curves show a near exact trend, verified by the near zero strain error. The size factor distribution is presented in Figure 3.14, showing the very random distribution of these new parameters throughout the thickness of the material, while the final dimensions of the UC and seven material layers are given in Table 3.1.

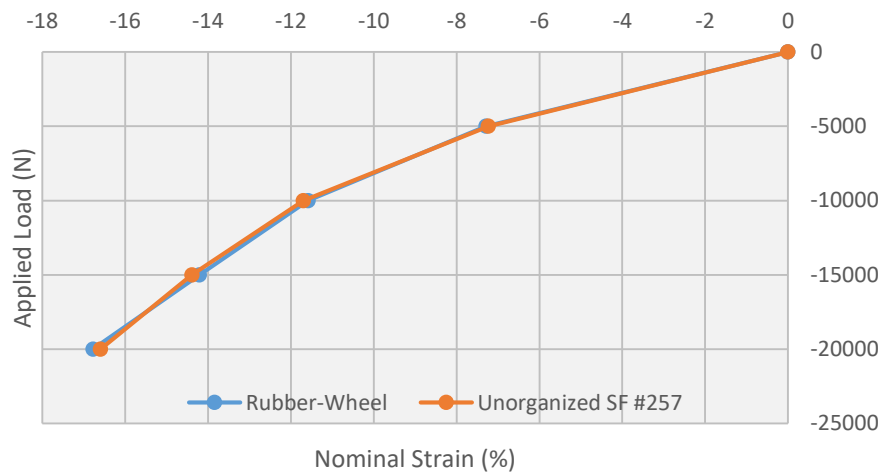


Figure 3.13 Mechanical Response of Meta-Band w/Unorganized SF

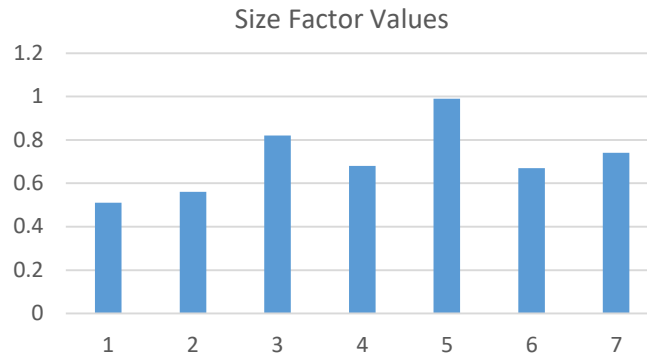


Figure 3.14 Layer by Layer Size Factor Distribution For Meta-band w/ Unorganized SF

Table 3.2 Optimal Design Parameters for Meta-band w/ Unorganized SF

Base Cell Geometries		Size Factors		Final CB Thicknesses	
T_2	1.16 mm	L1	0.51	Layer 1	0.592mm
θ_2	0.043 deg	L2	0.56	Layer 2	0.650mm
θ_3	0.654 deg	L3	0.82	Layer 3	0.951mm
		L4	0.68	Layer 4	0.789mm
		L5	0.99	Layer 5	1.148mm
		L6	0.67	Layer 6	0.777mm
		L7	0.74	Layer 7	0.858mm

Since all of the optimal designs were well within the limitations of the max stress for Ti-6Al-4V, the design with the lowest strain error was chosen as the final solution for the ‘meta-band’ design. Figure 3.15 shows this chosen design charted against the best designs from both the organized size factor optimization as well as the no size factor material optimization. The starting point for all three models is also shown to provide a reference for the amount of performance tailoring that is capable through the optimization process.

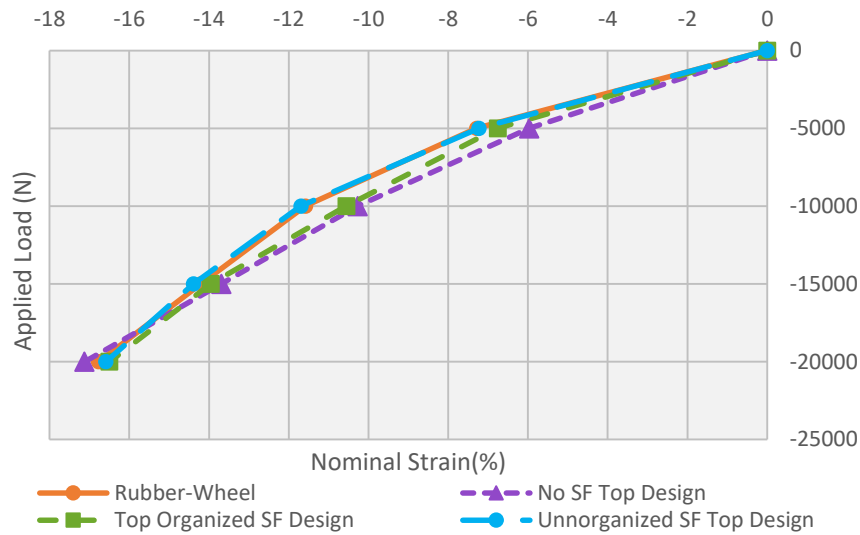


Figure 3.15 Mechanical Response of Meta-Band w/ Organized SF, Unorganized SF, and no SF

3.5. Conclusions and Discussion

Ultimately, the methodology used to design the circular meta-material for the tank road wheel provided an acceptable design that met the stringent constraints of the multi-objective optimization. Using the Modified Unit Cell Synthesis method to develop a meta-material in a completely different reference frame was an important test for the expanded implementation of the process. It also speaks to multiple environments that these cellular materials are well suited for. While it will take experimental validation of manufactured parts to confirm the predictive model, the favorable strain error results are very encouraging when compared to other meta-material optimizations.

Most importantly, however, was the observed success of the size factor addition, an idea that has the potential to drastically change the way these cellular materials are designed and the applications they are viable for. By breaking the trend of uniform materials in the x and y direction, the range of material performance for any given

configuration has been greatly expanded. This untapped design space of heterogeneous periodic meta-materials could fill even more nonlinear applications than initially thought possible.

CHAPTER 4. MULTI-LEVEL OPTIMIZATION OF TANK SYSTEM METAMATERIALS TRACK

4.1. System Approach

4.1.1. Single and Multi-Level Optimization

With confidence established in the feasibility of the canti-duo meta-band design, as well as the use of cell layer size factors for increased material variability, the next step was to investigate the combination and interaction of these meta-materials in the tank track system. When looking to optimize a system with more than one variable body such as this system, designers have some options in optimization that they can choose. In this case, the choice was between one single level or multiple levels approaches to meet the desired global and/or subsystem goals. Single level optimization utilizes the global targets desired of the system to obtain convergence, much like the optimization procedures discussed in previous sections. The respective behavior of individual subsystems contained within the larger system may be constrained to judge the success of a particular design solution; However, the optimizer is not actively seeking to improve specific independent behavior. It is only considering the final values. This type of optimization is suitable for problems that only need to meet a specific end target, and can be simpler to set-up and faster to run than a multi-level approach. Thus, in a search for answers to RQ2, the following, and last, research question was developed:

RQ2.3. Should a multi-level or single level optimization procedure be employed to design the system, and how do they compare with respect to final designs, convergence accuracy, and computational efficiency?

In systems where the behavior of the individual subsystems is critical to the overall success, multi-level optimization methods are better suited. Multi-level optimization usually applies to systems with a hierarchical structure, where optimal variables for a particular subsystem need to be determined and subsequently implanted into the higher level optimization, in order to determine some additional set of higher order variables [24][25]. These multi-level approaches are incredibly useful when trying to achieve multi-discipline performance objectives in complex mechanical or biological systems [26][27]. For example, in [28] a multi-level optimization of an internal combustion engine is carried out, highlighting a bi-level approach for the design of the combustion chamber. The results of lower level geometric and thermodynamic optimizations are gathered and input into the higher level system optimizer, providing a combustion chamber design and a new set of optimizable parameters.

In relation to the meta-material system, the difference between the single and multi-level optimization approaches lies with whether or not the individual material responses should mimic the response of their respective rubber counterparts. Additionally, the multi-level approach in this scenario would not have additional parameters that need to be solved for. Instead there is just a global convergence constraint that would determine when the optimizer can be stopped, but this will be touched upon more in Section 4.2.2. Figure 4.1 highlights the key points of both optimization approaches with respect to their considerations and final objectives for this particular meta-material system.

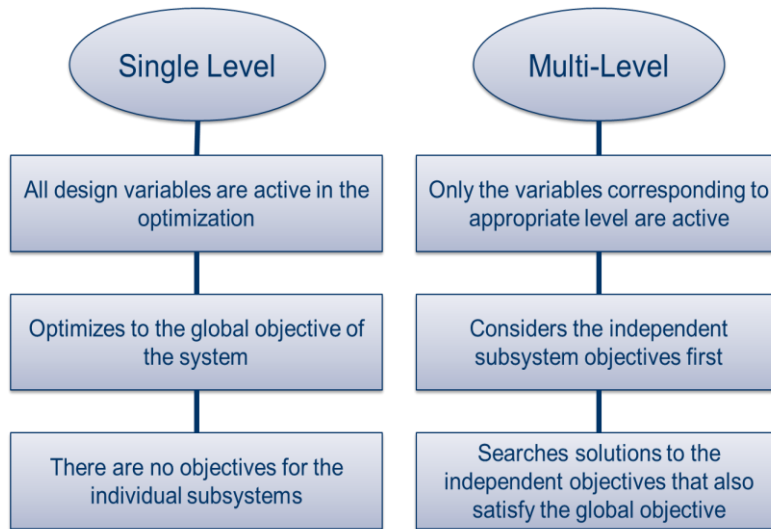


Figure 4.1 Comparison of Single and Multi-Level Optimization Methods for Metamaterial System

4.1.2. Target Gathering

Before either of the system optimizations can be carried out, the appropriate targets for each of the approaches must be identified. The rubber-rubber system exhibits a global response under loading, which is indicative of the overall suspension travel the tank or driver would experience. Regardless of the approach taken, this result is needed as the final convergence criteria. The rubber-rubber model can also produce the individual responses of the two components interacting with each other, providing three unique target responses and a much more complicated optimization procedure. These are generically visualized in Figure 4.2, with δ_W , δ_P , and δ_T representing the displacements of the wheel, pad, and total system respectively at the same particular point. Figure 4.3, on the other hand, shows a generic representation of the meta-material system for both single and multi-level, highlighting the respective deformations that each model would experience and how they will ultimately relate back to the targets obtained from the rubber-rubber model. The

objective strains are calculated from these displacement values using the ‘Meta_Strain’ equation from Table 1.1.

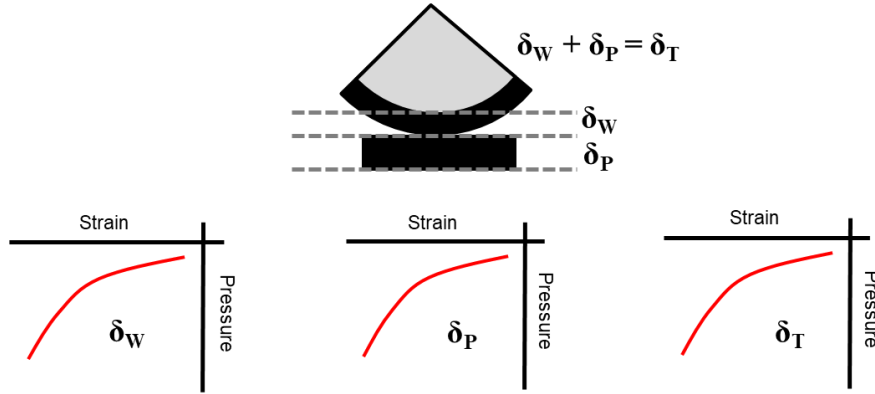
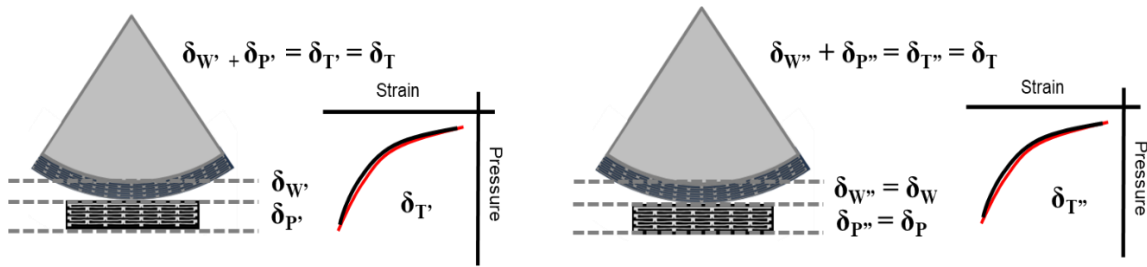


Figure 4.2 Representation of Rubber-Rubber Target Deformation Curves



**Figure 4.3 (Left) Single Level Optimization Target Deformation Curve
(Right) Multi-Level Optimization Target Deformation Curve**

Additionally, the rubber-rubber targets provide the deformations and subsequent objective strains for an additional and necessary optimization that lays the foundation for the eventual multi-level process.

In order to expedite finding the global system optimum, it is imperative that designers start as close to where they may believe said optimum is as they possibly can. This prevents the optimizer from becoming stuck in local minima and searching areas of the design space that are clearly infeasible. When using search algorithms such as NSGA-II, this need is not as important, since the optimizer occasionally mutates a design to ensure

exhaustive exploration of the design space. However, the use of more direct search methods, like the one proposed for the multi-level optimization, increases the chances of becoming trapped. It also decreases the amount of ground the algorithm has to cover before reaching the final solution, which reduces computational resources. By using the individual rubber responses as targets for optimization of the meta-material bodies, viable starting points can be obtained for the larger projects. Figure 4.4, shows a representation of the meta-materials interacting with their respective rubber opposites, such that the measured deformations, $\delta_{W''}$ and $\delta_{P''}$, match the original deformations, δ_W and δ_P , from Figure 4.2.

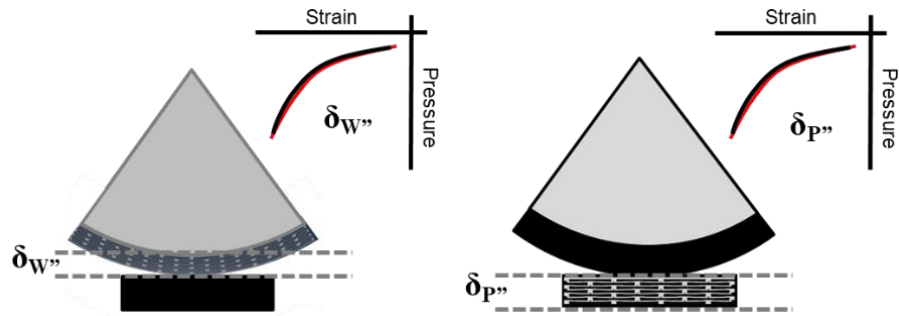


Figure 4.4 (Left) Meta-Band on Rubber Pad. (Right) Rubber-lined Wheel on Meta-Pad

A FE model of the rubber-rubber system was created and the overall target response, as well as the individual responses of the rubber components, were derived from it. The model puts both a rubber pad and wheel section in contact with each other. Three uniaxial points, with a vertical sliding condition, are used to constrain the deformation of the system, while the bottom of the rubber pad is fixed. Contact between the two bodies is defined by ‘hard contact’ for the normal behavior, which assumes zero penetration of one material into the other, and a penalty driven method for the tangential behavior, which uses a coefficient of friction to determine the nature of the interaction. The coefficient of friction

was set at 0.4, [8] and a second-order Ogden model was used to define the rubber material [8]. Figure 4.5 shows the three target curves. It is interesting to note that the deviation between strain percentages of the wheel and the pad is quite small, suggesting that the relative displacements of each body are the same. The pad and wheel strains are calculated based on their respective material thicknesses, while the total is calculated using the total thickness of the two materials prior to compression. The loads used to calculate those strains are the same loads used in the experimental testing ranging from 5kN to 22.5kN. Those strains can be found in Table 4.1, This will prove important in the multi-level optimization and determination of final geometries, as one body will not be able to account for most or all of the deformation.

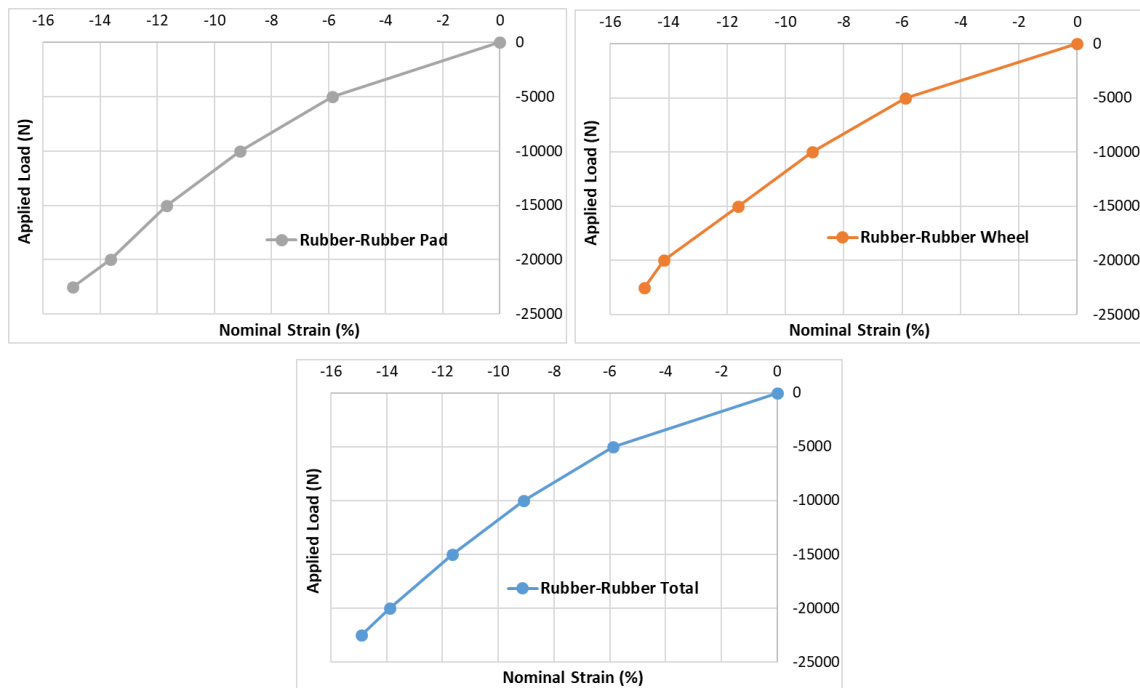


Figure 4.5 (Top Left) Pad Response in Rubber-Rubber. (Top Right) Wheel Response in Rubber-Rubber Model. (Bottom Center) Model System Response in Rubber-Rubber Model.

Table 4.1 Target Strains for Track System Rubber Components

Load (N)	Pad Strain (%)	Wheel Strain (%)	Total Strain (%)
-5000	-5.87	-5.90	-5.89
-10000	-9.09	-9.08	-9.08
-15000	-11.68	-11.63	-11.66
-20000	-13.63	-14.17	-13.88
-22500	-14.95	-14.83	-14.90

4.2. Multi-Level Optimization Procedure

While traditional multi-level optimization techniques insert the information obtained from the lower level into the upper level for a final optimization, the approach taken for this meta-system is slightly modified to accommodate the iterative loop embedded in the upper level. Figure 4.6 shows the entirety of the optimization levels and the general flow of information from level one to level two and within level two itself. The optimization starts with the redesign of the original backer pad, providing an initial design guess for the second level. Using two sub processes within itself, this second level exchanges results of embedded optimizations to form an iterative loop looking to satisfy both the subsystem and global-system objectives, described further in the next sections.

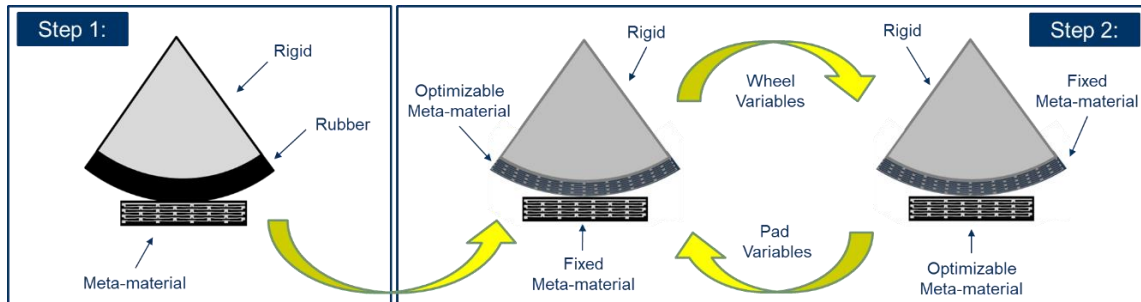


Figure 4.6 Diagram of Multi-Level Optimization Process

4.2.1. Step 1: Pad Reoptimization

To provide the appropriate initial guesses for the multi-level optimization, the initial pad needed to be revisited and reevaluated to better reflect the interactions it would be experiencing. By incorporating the wheel structure into the pad model, and incorporating contact settings and additional boundary conditions, the pad could be reoptimized and provide variable values closer to an eventual optimal system solution. This also makes the process more efficient by narrowing the design space eligible for search. Additionally, since the original pad had only been optimized in the simplified simulation environment, it would provide consistency from step one to step two in this multi-level procedure. The new model setup is highlighted in the diagram of step 1 of the multi-level approach, shown in Figure 4.7.

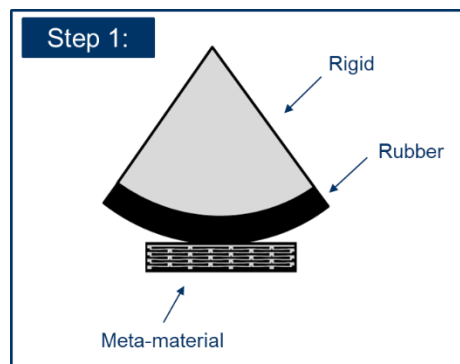


Figure 4.7 Step 1: Pad Reoptimization for Multi-Level Optimization

Given this need for pad reoptimization and the success of the size factor implementation for the ‘meta-band’ optimization, the thought of redesigning the backer pad using size factors was presented as a way to further validate the new parameters, while expanding the feasible design space. As discussed in the original case study, the ‘canti-oval’ pad design was selected, in part, because it provided the greatest percentage of real

and feasible design solutions. That particular pad design, however, incorporates slightly more complicated geometric features, such as the oval beams, that can cause problems in manufacturing, as documented in Chapter 2. By simplifying the pad design to the ‘canti-duo’ UC configuration and adding the size factors to each cell layer, the initial design could be revitalized and a new more robust pad design found.

4.2.2. Step 2: Bi-Level Iterative Loop

Following the reoptimization of the backer pad, the optimization of the meta-material system is initiated in step two’s two-level iterative loop. Unlike traditional multi-level systems, which have a hierarchical structure, this step is designed to use two levels of the same rank to systematically progress towards an optimum. For this step, a new FE model was created and used, including both meta-material bodies in interaction with each other. The same model would be used for both lower level optimizations, with distinctions made in each optimization procedure for fixed and changeable variables. This ensures consistency between the interactions and eventual outputs of the two procedures.

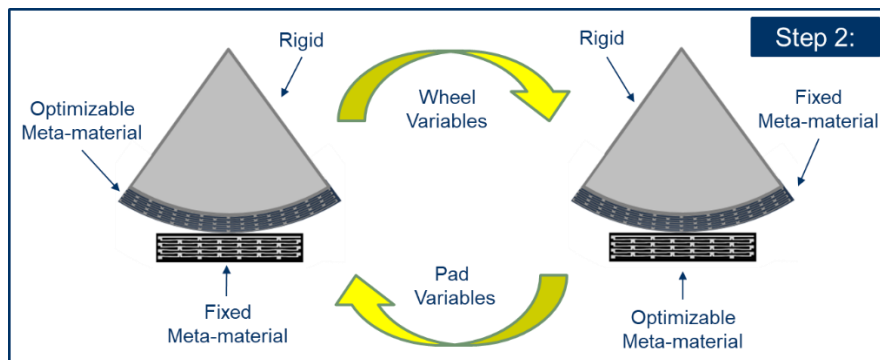


Figure 4.8 Step 2: Iterative Loop for Meta-material System Optimization

4.2.3. Considerations for Optimization in modeFrontier

To utilize modeFrontier for this complicated optimization problem, special considerations needed to be taken to ensure the successful gathering of outputs and transfer of inputs. The project files used in the previous single material optimizations, such as the ‘meta-band’, are not capable of being modified to handle the entirety of this new method. Upon consulting with ESTECO, it became apparent that no single workflow could be created to handle the whole project, and that multiple nested and interconnected projects would be needed to generate the greater project.

Looking at step one, the reoptimization of the backer pad follows the same methodology as the previous single material optimization projects. Given their similarities, repurposing those original files, with modifications to input parameters, the specific FE model analyzed, and outputs requested, was a viable option. Step two, however, would prove more difficult to sort out. At its core, the step two optimization loop utilizes the same thought process as previously discussed. Fixing the design variables of one material turns the problem into a single material optimization with a single design objective. This can be said for both the pad and wheel optimization within step two. Therefore, old files once again provide the appropriate template for these lowest level optimizations. The iterative loop, however, requires the passing of information from one file to the next. This requires the implementation of a single iteration linear process, available in the modePROCESS add-on of mF, shown in Figure 4.9.

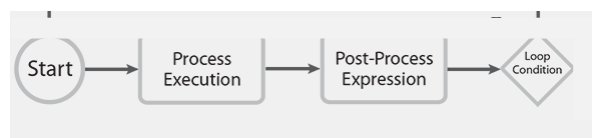


Figure 4.9 ModeFRONTIER Loop Diagram for Multi-Level Optimization

This single run process outlines the flow of information from the first optimization (sub-process) of the loop to the second and assigns the output data of the first sub-process to the appropriate input parameters of the second sub-process. This single loop also organizes the output data of the second sub-process into a sorted table for the optimizer to choose the most ‘optimal’ design from. To introduce a termination criteria check and the multiple iterations, like Figure 4.6 suggests, a third layer was needed to recirculate the optimal design back to the beginning of the loop and also to set the target values for project termination. This upper most level resulted in an updated loop diagram, shown in Figure 4.10, and a submission ready template for a multi-level system optimization.

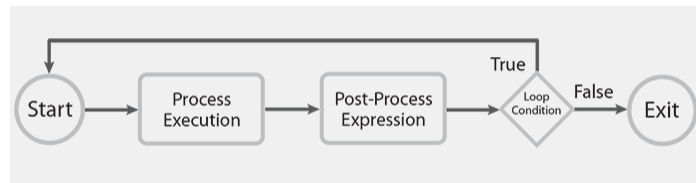


Figure 4.10 Updated ModeFRONTIER Loop Diagram for Multi-Level Optimization

4.3. Canti-Duo Backer Pad - Rubber Wheel Optimization

The initial step of the multi-level approach calls for the optimization of the original meta-material backer pad, with those optimal pad variables acting as an initial guess for the DOE of the second phase. To complete this optimization, modifications were made to the previous ‘meta-band’ project files. While most changes were small adjustments to objective or constraint values, the introduction of a modified pad design was by far the most important alteration made for this particular problem. The success of the size factor implementation provided a remarkable increase in nonlinearity control in the ‘meta-band’

optimization. In an effort to further size factor implantation, provide increased validation of their effects, and simplify the backer pad design for manufacturing, a ‘canti-duo’UC configuration was reimplemented as the foundation of the pad, with size factors added as additional parameters. Therefore, a secondary goal of this optimization is to determine if the inclusion of these additional variables can provide increased control over the mechanical behavior of the pad and subsequent, feasible design solutions.

The new FE model placed the backer pad in contact with a rubber lined road wheel to ensure consistency with the actual environment of the track system. Contact was introduced between the outer surface of the road wheel and the top surface of the pad, defining both a normal and tangential contact behavior for the system. The same “hard contact”, as defined by the previously described rubber-rubber model, was used for the normal behavior, and the same penalty method, using a coefficient of friction of 0.4, defines the tangential behavior [29][8]. The original boundary conditions of the backer pad model were replaced with conditions more reflective of the system, with the bottom of the pad fixed and three coaxial points chosen for a sliding constraint in the y-direction. This final boundary condition would ensure deformations only occurred in the y-direction. Figure 4.11 shows the configuration of the model. Upon creation and insertion of this new FE model, the optimization was run. Table 4.2 show the objective functions and target constraint values used to determine success of the designs. A Uniform Latin Hypercube was chosen as the source for the initial DOE, with the boundaries for the DOE corresponding to the geometric limitations for part generation and meshing in the FE solver.

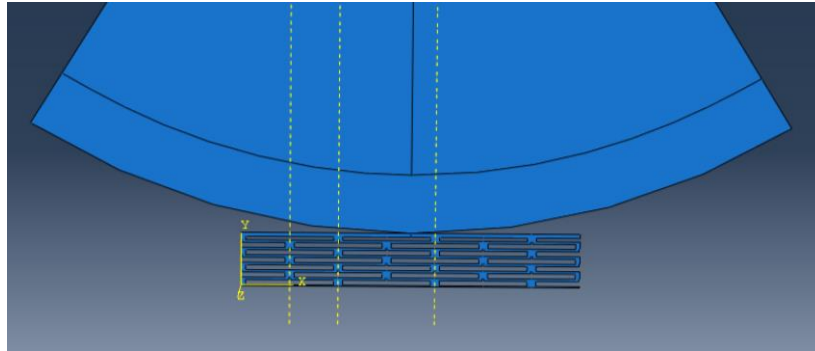


Figure 4.11 FE Model of Canti-Duo Pad and Original Track System Road Wheel

Table 4.2 Backer Pad Reoptimization Objectives & Constraints

Objectives	$\text{Min: } f = \sum_{i=1}^4 \varepsilon_{P'} - \varepsilon_P ^2$ $\text{Min: } g = \sigma_{MisesMax}$
Variable Definitions	$\varepsilon_{P'} = \frac{\delta_{P'}}{H_{MetaPad}}$ $\varepsilon_P = \frac{\delta_P}{H_{RubberPad}}$
Constraints	$\sum_{i=1}^4 \varepsilon_{P'} - \varepsilon_P ^2 \leq 7.5E^{-5}$ $\sigma_{MisesMax} \leq 9.0E^8$

After 300 evaluated designs, the optimization procedure was determined to have reached convergence on the global minimum, with more than 50% of the evaluated designs meeting the desired output constraints. This is shown in the design summary chart depicted in Figure 4.12, while a scatter chart of the evaluated designs, in Figure 4.13, clearly outlines the Pareto tradeoff of the feasible design space. The pareto designs are outlined in red along the bottom left of the chart.

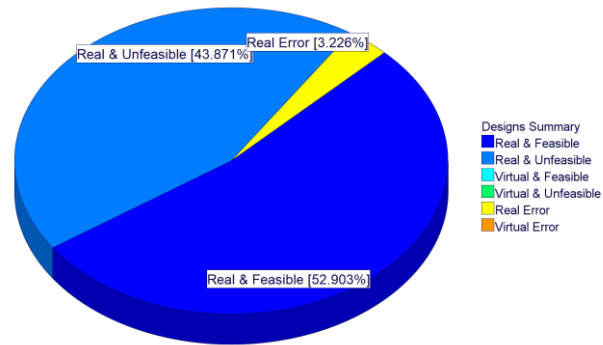


Figure 4.12 Canti-Duo Backer Pad & Rubber Wheel Design Summary Chart

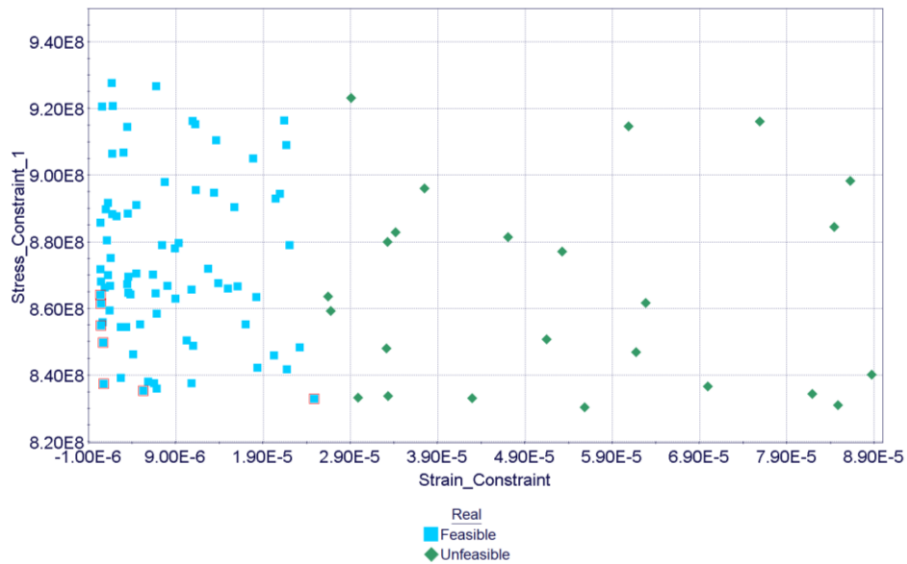


Figure 4.13 Canti-Duo Backer Pad & Rubber Wheel Design Chart

Figure 4.14 shows the mechanical response of the most optimal pad design compared to the target response of the rubber pad compressed by a rubber wheel. Falling well below the target, this result is the smallest strain error obtained during any meta-material optimization. Additionally, these results further document the successful use of size factors in expanding the feasible design space for these nonlinear meta-materials. In fact, when compared to the original case study, implementing size factors resulted in more than a 1000% increase in feasible designs.

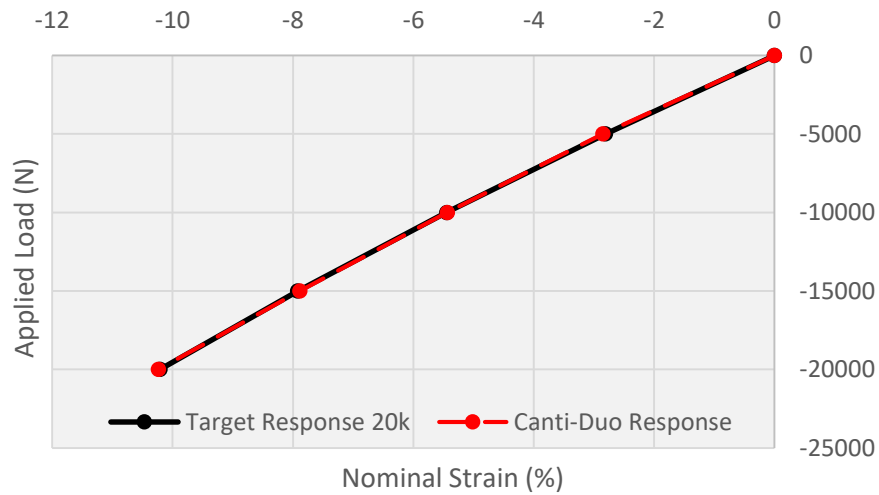


Figure 4.14 Mechanical Response of Reoptimized Canti-Duo Pad

Lastly, Figure 4.15 shows the profile of the pad with the visible effects of the size factors. The variances in cantilever beam thickness are clearly visible and highlight the amount of change these size factors are capable of imparting. Additionally, the list of final design parameters, including size factors are shown in Table 4.3 and the bar chart in Figure 4.16 provides a graphical representation of the size factor distribution, from layer to layer.

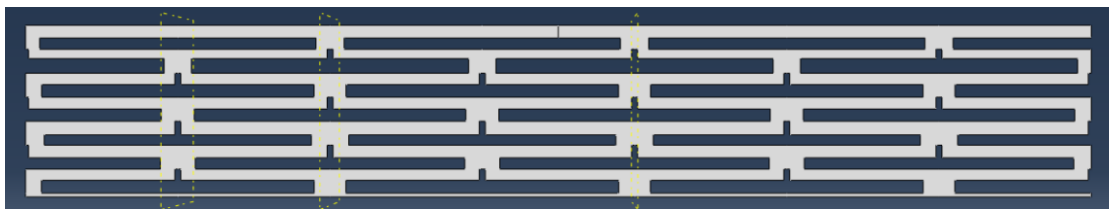


Figure 4.15 Profile of Canti-Duo Pad Final Design

Table 4.3 Optimal Design Parameters for Canti-Duo Backer Pad

Base Cell Geometries		Size Factors		Final Thicknesses			
T₂	1.94 mm	L1	0.77	L1 * T₂	1.49mm	L1 * T₃	1.73mm
T₃	2.25 mm	L2	0.87	L2 * T₂	1.69mm	L2 * T₃	1.96mm
Gap	0.12 mm	L3	0.94	L3 * T₂	1.82mm	L3 * T₃	2.12mm
		L4	0.81	L4 * T₂	1.57mm	L4 * T₃	1.82mm
		L5	0.78	L5 * T₂	1.51mm	L5 * T₃	1.76mm
		L6	0.64	L6 * T₂	1.24mm	L6 * T₃	1.44mm

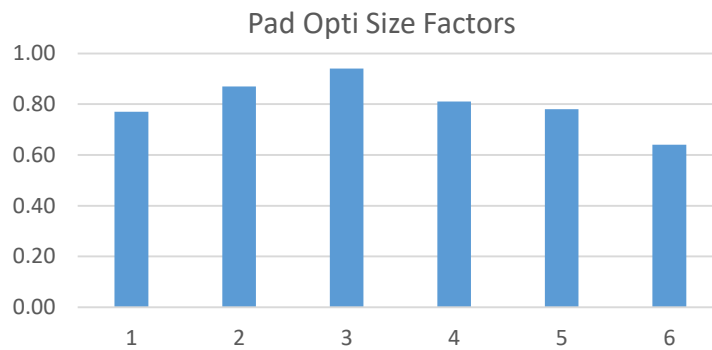


Figure 4.16 Canti-Duo Backer Pad Distribution of Size Factors

4.4. Multi-Level Optimization Results

The multi-level optimization was submitted using a three level modeFrontier optimization program, designed to run until a criteria matching design was obtained or 10 total iterations of the step 2 loop were run. At the lowest level, two scheduling project utilized the NSGA-II algorithm to systematically search 50 designs, and sort them by strain error of either the pad or wheel meta-material, depending on the stage of the loop. Upon sorting the results of the second scheduling projects, the strain errors of the pad and wheel are extracted, added together, and compared against the termination criteria of the largest level. If the value is low enough, the loop is stopped and the design variables of that scheduling project are extracted. If the error value is larger than required, the output

variables of the second project as the fixed variables in the first project of the next iteration. The objectives and constraints of the lowest level projects, as well as the termination criteria of the top level are presented in Table 4.4

Table 4.4 Multi-Level Optimization Objectives, Constraints, & Termination Criteria

Wheel Optimization Objective	$\text{Min: } f = \sum_{i=1}^4 \varepsilon_{W'} - \varepsilon_W ^2$
Wheel Optimization Constraint	$\sum_{i=1}^4 \varepsilon_{W'} - \varepsilon_W ^2 < 3.0E^{-5}$ $\sigma_{MisesMax} \leq 9.0E^8$
Pad Optimization Objective	$\text{Min: } g = \sum_{i=1}^4 \varepsilon_{P'} - \varepsilon_P ^2$
Pad Optimization Constraints	$\sum_{i=1}^4 \varepsilon_{P'} - \varepsilon_P ^2 < 3.0E^{-5}$ $\sigma_{MisesMax} \leq 9.0E^8$
Top Level Termination Criteria	$\sum_{i=1}^4 \varepsilon_{W'} - \varepsilon_W ^2 + \sum_{i=1}^4 \varepsilon_{P'} - \varepsilon_P ^2 < 7.0E^{-5}$

Like other optimizations, a Uniform Latin Hypercube was used to determine the initial DOE for the first iteration, as well as the DOE for each successive iteration. The details of the model, with regards to contact interaction definitions and parameters and boundary conditions, are the same as the model details for the rubber-rubber and pad reoptimization models. This maintains consistency between the results of all the related models. The entire process was then put on the Palmetto cluster supercomputer to run for

a maximum of three days, as allotted by usage regulations. Upon reaching the three-day limit, the optimization procedure was halted, with six full iterations of the step 2 loop completed. With each loop running two scheduling projects, both running 50 designs a piece, each iteration of the loop took roughly 11 hours to complete. Since the optimization had to be stopped, no ‘real and feasible design was found. If so the process would have terminated. However, since the optimization was single objective, the output design variables of iteration six could be observed as the most optimal design found. Extracting the corresponding strain values, the behavior of the subsystems and global interaction were graphed against the target curves. Figure 4.17 shows the curves of the pad and wheel mechanical responses compared to the target values. The strain values obtained, and the corresponding error values, are displayed in Table 4.5. Figure 4.18, on the other hand, shows the global response of the system compared to the rubber-rubber system. The system strain values and strain error are also listed in Table 4.5.

Table 4.5 Multi-Level Optimization Subsystem & Global Strain Values

Load	Pad Target	Pad Result	Wheel Target	Wheel Result	Total Target	Total Result
-5000	-5.87	-6.77	-5.90	-4.66	-5.89	-5.75
-10000	-9.09	-9.52	-9.08	-8.38	-9.08	-8.97
-15000	-11.68	-11.84	-11.63	-11.72	-11.66	-11.78
-20000	-13.63	-14.09	-14.17	-14.81	-13.88	-14.44
Error	3.36E-04		1.01E-04		3.59E-05	

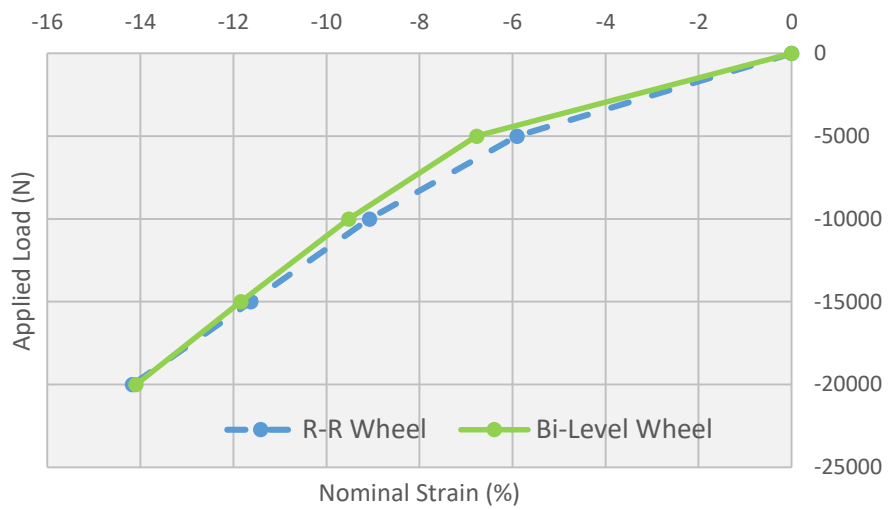
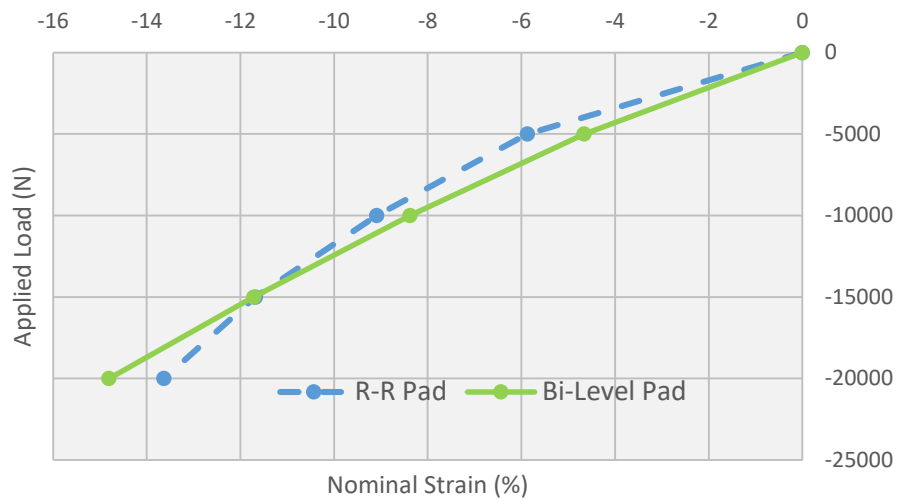


Figure 4.17 Bi-Level Optimization Subsystem Mechanical Responses

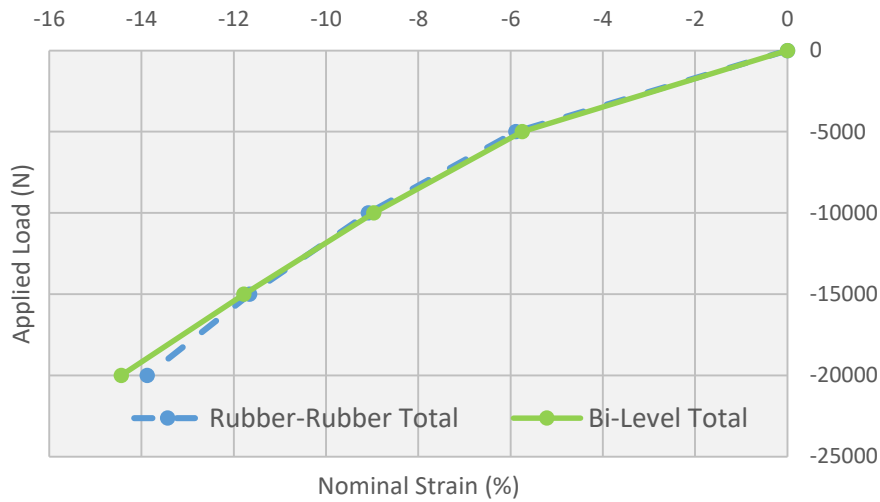


Figure 4.18 Bi-Level Optimization Global Mechanical Response

The goal of the multi-level optimization was to obtain meta-material pieces that behaved in near exact accordance with the rubber pieces they are designed to replace. By obtaining two pieces with acceptable strain values, the global response of the system would, by default, correspond with the rubber-rubber system response. While the subsystem responses are well outside the desired strain error range, the total response showed a passable fit to the target response. Unfortunately, the maximum stress of the two materials is approaching the yield stress of the bulk material. The inclusion of fillets and further refining of the model mesh, however, could reduce or correct the high strain values to more acceptable values. The final design variables of the two meta-materials are listed in Table 4.6 and a bar chart of the size factors, similar to other optimizations, is shown in Figure 4.19.

Table 4.6 Multi-Level Optimization Optimal Design Variables

Pad Size Factors		Pad Base Geometry		Wheel Size Factors		Wheel Base Geometry	
L1	1.06	T2	1.79	C1	0.54	T2_W	1.03
L2	0.5	T3	2.26	C2	0.88	Theta2	0.075
L3	0.79	Gap	0.1	C3	0.84	Theta3	0.668
L4	0.94			C4	0.73		
L5	0.59			C5	1.07		
L6	0.9			C6	0.58		
L7	0.65			C7	0.80		

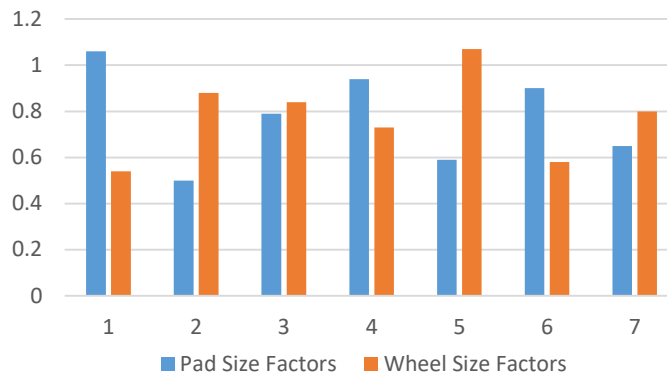


Figure 4.19 Multi-Level Optimization Size Factor Distribution

4.5. Single Level Optimization Set-up & Results

The basics for the single and multi-level approaches are rooted in multi-objective optimization, but the single level method presents a unique advantage over the multi-level with a less complex web of input and output transfers. With all the variables active, the single level project could be conducted by repurposing the optimization workflows from the multi-level sub-process optimizations. The only significant adjustments that needed to be made were the activation of the remaining input parameters, the implementation of the FE model combining the two meta-material parts, and updating the appropriate outputs from the FE model. Having this uniform program with the ability to add, remove, or change

the small details of the particular optimization run is a huge advantage and drastically cuts the time required to troubleshoot programs created from scratch.

While the multi-level optimization method looks to iteratively search for the meta-material designs that will meet both the global strain objectives of the entire rubber-rubber system and the independent strain targets of the rubber pieces, the single level approach looks to obtain a system design constrained solely by the global performance of the two parts. The diagram in Figure 4.20 reviews the target and measured displacements for the single level approach, while the chart in Figure 4.21 shows the objective response curve, with the four loadings increments.

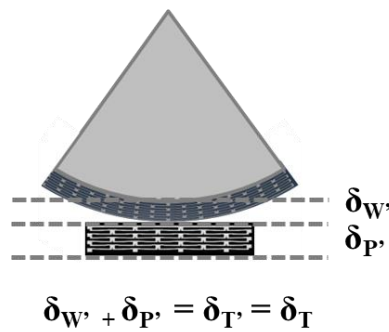


Figure 4.20 Measured Displacements of Single Level Optimization

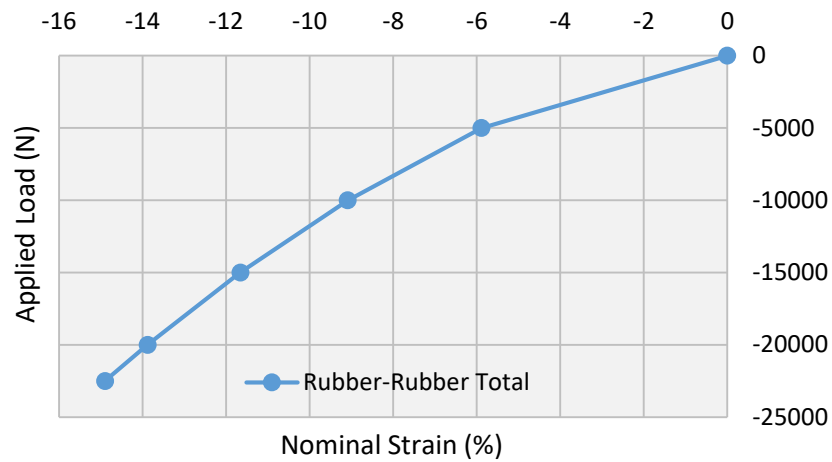


Figure 4.21 Target Response of Rubber-Rubber Track System

Upon supplying the optimizer with the necessary new information, the single level program was submitted to the Palmetto high performance cluster to run. Similar to previous optimizations, NSGA-II was used to search the design space and a Uniform Latin Hypercube was used to establish the primary DOE. The two objectives reflect those used in previous runs, with the first objective being to minimize the strain error between the target and model system responses and the second being to minimize the maximum stress experienced within the system. Two constraints, also similar to those used in previous optimizations, were employed to determine which designs were considered successful in the eyes of the optimizer. The objectives and their respective constraints are shown in Table 4.7.

Table 4.7 Single Level Optimization Objectives & Constraints

Objectives	$\text{Min: } f = \sum_{i=1}^4 \varepsilon_{T'} - \varepsilon_T ^2$ $\text{Min: } g = \sigma_{MisesMax}$
Variable Definition	$\varepsilon_{T'} = \frac{\delta_{T'}}{H_{Wheel} + H_{Pad}}$ $\varepsilon_T = \frac{\delta_T}{H_{RubberWheel} + H_{RubberPad}}$
Constraints	$\sum_{i=1}^4 \varepsilon_{T'} - \varepsilon_T ^2 \leq 2.5E^{-5}$ $\sigma_{MisesMax} \leq 9.0E^8$

Convergence for this single level optimization was reached after 300 evaluated designs, after which the procedure was halted. However, given the defined constraints, none of the tested designs succeeded in besting, or meeting, the desired values. As seen in the design summary chart, Figure 4.22, 100% of evaluated designs are accounted for as either real errors or real and unfeasible solution. What this chart does not account for is whether or not one or both of the objectives was not satisfied. A design will not return feasible if all constraints are not achieved. But, in the case of these meta-materials, failure to meet the strain objective will result in undesirable performance while failure to meet the stress constraint will result in a broken pad. By examining Figure 4.23, which shows the objective values for each design, a concentration of designs can be seen placed below the stress constraint, but above the strain constraint, making them physically feasible designs with larger than desired error.

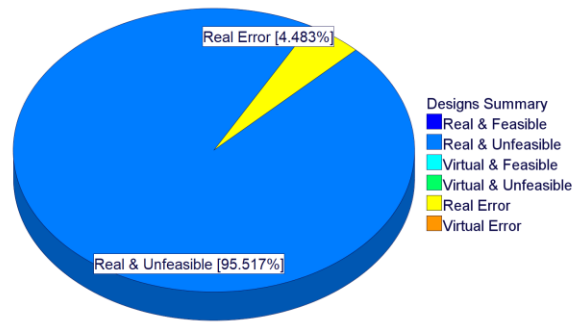


Figure 4.22 Design Summary Chart of Single Level Meta-material Optimization

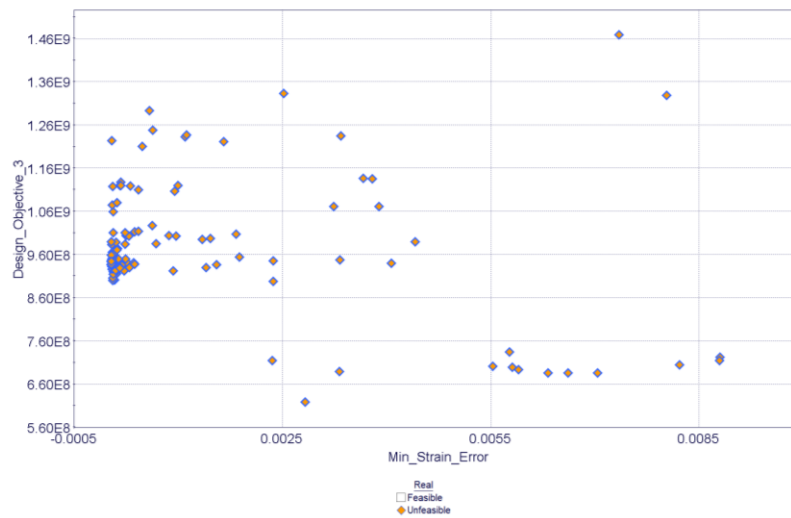


Figure 4.23 Design Objective Scatter Chart of Single Level Meta-material Optimization

Despite none of the designs meeting the desired strain error, when the constraint value is increased by 10%, several designs become eligible as real and feasible solutions. Since the objective is to minimize strain error, with the constraint value determining the relative success, the mechanical behavior of the design presenting the smallest error is charted against the target response. In addition, the responses of the individual materials in the system were charted against their respective rubber counter parts. This provides a complete picture of the meta-material system behavior, both at the global level and the

subsystem level, and a viable comparable to the multi-level results. These charts are shown in Figure 4.24 and Figure 4.25. Table 4.8 provides the numerical strains for both the subsystems and global system

Table 4.8 Single Level Optimization Subsystem and Global Strain Values

Load	Pad Target	Pad Result	Wheel Target	Wheel Result	Total Target	Total Result
-5000	-5.87	-6.40	-5.90	-4.62	-5.89	-5.47
-10000	-9.09	-10.49	-9.08	-7.57	-9.08	-8.96
-15000	-11.68	-13.73	-11.63	-9.82	-11.66	-11.69
-20000	-13.63	-16.64	-14.17	-11.85	-13.88	-14.14
Error					2.59E-05	

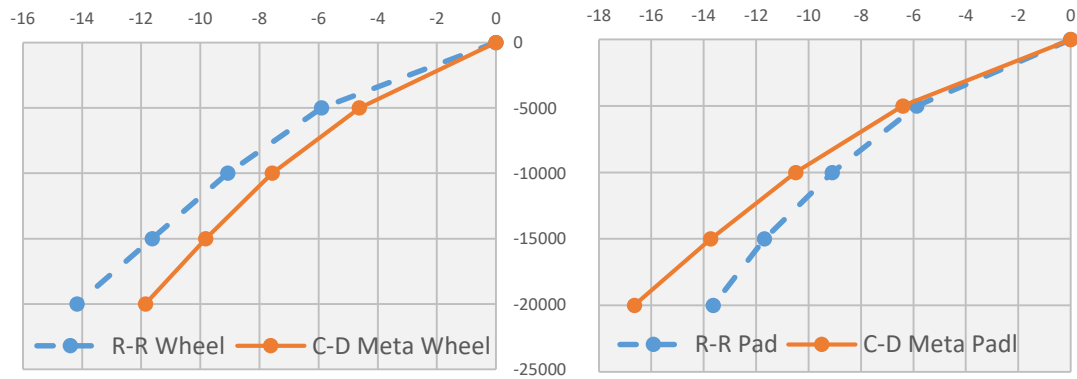


Figure 4.24 Single Level Optimization Mechanical Responses of Meta-material Subsystems

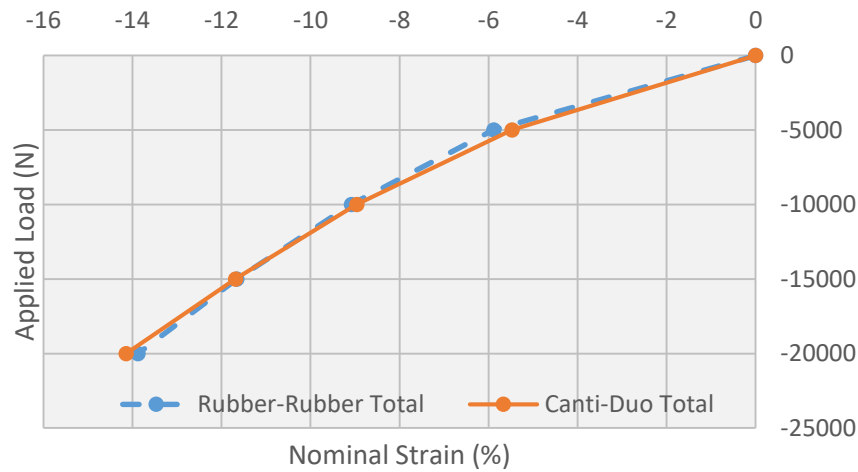


Figure 4.25 Single Level Optimization Mechanical Response of Meta-material System

What is interesting about these results is that the subsystems display large disparities between their responses and their respective rubber counterparts' responses, despite the global system response closely matching the desired curve. This apparent averaging of subsystem behavior is a useful revelation for future designing, especially in situations where the highest level mechanical response is the only pertinent target. This presents the possibility of many feasible final design solutions, so long as the average deformation of the two materials resembles the target response. In the case of the track system, designers could even replace one of the meta-materials with a more rigid material, i.e. steel, and tailor the deformation of the second material to account for the entire target system's behavior. If secondary targets were to change or additional targets were to be added, this observed averaging presents designers with newfound flexibility to address them while continuing to meet the primary objective. Lastly, since size factors were included in both of the meta-materials, the bar chart in Figure 4.26 shows the layer by layer

breakdown of both materials, while the final parameters of the entire system are provided in Table 4.9. The chart reinforces the seemingly random nature of their organization

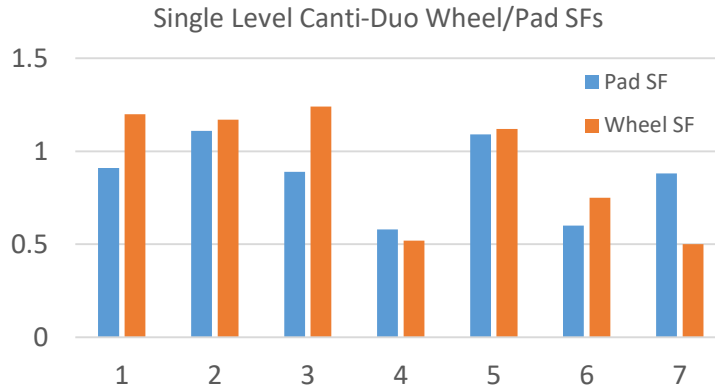


Figure 4.26 Layer by Layer Breakdown of Meta-material Size Factors

Table 4.9 Final Design Parameters from Single Level Meta-material Optimization

Size Factors - Wheel		Size Factors - Pad		Unit Cell Base Geometries			
C1	0.91	L1	1.20	T _{3_P}	1.95mm	T _{2_W}	1.24mm
C2	1.11	L2	1.17	T _{2_P}	1.30mm	θ ₂	0.047°
C3	0.89	L3	1.24	Gap_P	0.51mm	θ ₃	0.308°
C4	0.58	L4	0.52				
C5	1.09	L5	1.12				
C6	0.60	L6	0.75				
C7	0.88	L7	0.50				

4.6. Comparison of Results and Discussion

When looking to compare the results of the multi-level and single level optimizations, the initial choice appears to be the clear. The single level results show favorable matching for the global system target, while the subsystem responses vary drastically from their rubber counterparts. The results of the multi-level optimization provided designs that failed to meet both the global response and the subsystem responses, however the error value for the global target was not far off from the single level results.

However, in terms of explicitly meeting constraints and the overall process objective, no viable solution could be found. It appears that as the subsystem designs whittle closer to the constraints, they are influenced by the interaction with and the behavior of each other. Additionally, one material seems to dominate the general behavior pattern of the system, something that could also be preventing the last bit of convergence of both meta-materials in the multi-level system. This could make it increasingly difficult to find two material designs that complement each other's behavior, while also meeting their individual needs. On the other hand, the averaging of the single level can take two drastically divergent subsystem responses to converge on the global, making it the more feasible method for the subsystem design. It even takes two materials of vary nonlinearity to combine and achieve the desire level of stiffening. By using two materials that can assume a broader range of behaviors with implemented methods for increasing or decreasing the nonlinearity, as opposed to meeting two small target ranges somewhere in the middle, it is not surprising that the single level offers more advantages.

Particularly intriguing is the opposite responses observed by the set of subsystems for the two optimizations. For the multi-level, the wheel material exhibited less stiffening, while the pad showed a greater degree of stiffening. Additionally, the wheel behavior tended to undershoot the desired strains and the pad tended to overshoot the strains. When looking at the behavior of the single level results, the opposite is true. The wheel experienced the larger stiffening trend, while mainly overshooting the strains. The pad showed more linearity in its behavior, and undershot the strains up to 15kN. When combined with the fact that the size factor distributions of the two optimizations show no

correlation between each other, this result shows the variability of these materials when these factors are implemented

This final choice between methods is dominated primarily by the computational requirements and overall strain value obtained in the given results. The multi-level optimization is set-up to terminate after 10 loops or upon discovering a real and feasible design. Because this is a more direct search method, using a single objective to judge each design, the process can terminate upon discovery. The single level approach uses a genetic algorithm to search the design space for a determined number of designs and is not stopped until the designer dictates or the last design is reached. If the multi-level approach were to discover the termination design, then it is possible that it's computational time would be less than the single level. However, if the termination design isn't found, the multi-level approach takes more than three days to run until loop termination. That is using the current system model. The single level approach takes roughly 30 hours to run 300-350 designs, the mark where convergence was obtained for this particular optimization. Therefore, in regards to time to convergence, the single level approach wins again. There are potential methods to decrease the searchable design space for the multi-level approach, such as dynamically adapting limits to the design as loop count increases. This will be touched upon more in Chapter 5.

Lastly, both methods take the same amount of computational resources to run, and both can be scaled up or down according to available resources. But what is interesting to note is the amount of time that was required to set-up and troubleshoot the far more complex multi-level method. The nested workflows are difficult to dissect and the sheer

volume of intra-model connections and data transfer leaves designers susceptible to making mistakes that lead to operational errors. While the template becomes much easier to manage after successfully running the first time, appropriate time should be allocated when building an optimization program like this.

Ultimately, the final choice should be dictated by the designer's needs. The time commitment to the multi-level is less of a concern if the need for subsystem matching is required, and the results cannot rule out that the multi-level optimization would reach an ideal design, provided more time on the high performance cluster.

CHAPTER 5. CONCLUSIONS AND FUTURE WORK

5.1. Conclusions

Overall, the work presented in this thesis looks to address the research questions presented, while also attempting to conclude the initial backer pad investigation and begin a larger study of multiple meta-materials interacting with each other.

In Chapter 2, RQ1 looks to discover the mechanical behavior of the additively manufactured meta-materials from previous work. Using both compressive and fatigue testing, comparisons could be drawn between the computed responses of the FE model and the physical behavior of the titanium pads. Upon running both tests, the numerical and experimental results showed significant differences between them. In static compression, the experimental results showed the pad behaved significantly softer, roughly 2.5 times, than expected. Similarly, the fatigue results also showed tremendous deviation from the predicted life of the pad. This comes as less of a surprise, however, as fatigue behavior is directly dependent on the amount of displacement experienced during compression. With higher strain values at the desired loads, the strains experienced in each cycle of the fatigue test are larger as well. This could account for some of that deviation

The deviation observed during the compression testing is a larger problem that must be addressed at the root causes. Three potential sources of deviation are suggested as factors in the discrepancies. Systematic analysis shows that all three of the sources have the capacity to significantly effect the behavior of the model and suggest that a softer than expected manufactured pad is not out of the question. It is, therefore, important to implement these types of analyses on these materials that are desperately dependent on the

dimensional values of its interior geometries. This could also open the door for more efficient designing of these favorable cellular materials, by identifying design trends that are less susceptible to manufacturing error and intra-variable interaction.

Chapter 3 begins with an attempt to answer RQ2, concerning a meta-material system design. However, two additional questions were required to sufficiently determine that answer. Addressing RQ2.2, the implementation of size factors proved to be an incredibly effective method for expanding the level of control that designers have over the characteristic behavior of these materials. Additionally, these size factors added to the overall Modified UCS method, providing a new layer of design parameters and adding an additional consideration to the overall methodology. With this promising answer to RQ2.2 comes the crucial answer to RQ2.1. In order for the system optimization to proceed, a feasible design had to be obtained for the meta-band portion. With size factors providing the desired improvement to material behavior, a promising meta-material design solution and successful answer to RQ2.1 was achieved. This successful design provided confirmation that additional applications, particularly in the nonlinear reference frame, are an achievable goal using these meta-materials.

Chapter 4 presented the last of the secondary research questions, RQ2.3, aimed at discerning the ideal method for designing and optimizing these meta-materials. Upon completion of both optimization procedures, the single level method emerged as a strong candidate for the system design. While the multi-level approach has idyllic goals for both subsystem and global convergence, the lack of attainability for either leaves the method infeasible. The single level approach, on the other hand, provides suitable curve matching

to the target response and offers a secondary additional benefit with respect to the final set of feasible solutions. Since the single level approach appears to average the responses of the two materials to achieve the target, a larger group of material behaviors may prove suitable for these types of optimizations. So long as the subsystem targets are not the primary objective, global objective convergence appears to be much more obtainable. This result also definitively answers RQ2. A viable meta-material system can be designed using Modified UCS methodology.

However, from the convergence aspect, it is not possible to definitively pick an ideal method. Since the multi-level approach was terminated before the global 10 loop iteration limit was met, it is possible that an optimal solution is available in the design space and just needs more time to be found. The termination was solely determined by the high performance cluster's single job time limit.

Lastly, running two additional models, one single level and one multi-level, with slightly modified target outputs and constraints could provide more definitive insight into the success of each method. Using multi-level search for a design solution to only the global target would provide a more analogous comparison to the current single level and determine which method should be employed definitely for a global system design. Using a constrained single level to search for a subsystem and global matching design would provide the most complete look at the capabilities of both methods in the regards of matching both levels, and again, provide more a more definitive conclusion.

5.2. Future Work

5.2.1. Backer Pad Experimental Testing

Due to a lack of available parts, experimental testing of the backer pads was limited to one physical specimen. Unfortunately, that one pad suffered critical failure during the fatigue portion of the testing. Additional work and additional pads are needed to rigorously test the mechanical behavior of this particular design. While the initial results are telling, it is only one data point, and more test are needed to ensure the quality of the first print and establish a consistent expectation for the manufactured pieces. Additionally, more pads would provide the opportunity to destructively measure the interior geometries of the pads. This could reveal patterns in the manufacturing, such as consistent under/over printing certain dimensions or the integrity of the prints throughout the entire z-axis of the part.

More pads would also provide the opportunity to expand the fatigue testing, not only running additional tests at the original load ratio, but also running tests at a reduced max strain value. Using strains on par with those predicted by the fatigue model can provide consistency between the experimental and model environments, as well as the eventual results. That is, assuming the strain deviations hold true in future batches of pads.

Lastly, additional prints would provide the opportunity to print tensile testing specimens for material property analysis and validation. While the manufacturers provide their own batch data, many printing process parameters can affect the final results, as discussed previously in the paper. By printing these specimens in multiple orientations and in the same bed batch as the pads, the most accurate material property data can be obtained

and a deeper understanding of optimal print parameters for these cellular materials may be achieved. Print directionality observations can also be made with the pads, by changing the orientation of the part in the bed, helping to identify a more detailed set of material property values that can then be inserted into the models for even greater fidelity. When combined with experimentally obtained density parameters, the most accurate depiction of the backer pad can be modelled and optimized.

5.2.2. Sensitivity Analysis for Meta-material System

As suggested at the end of Chapter 2, the sensitivity analysis conducted on the dimensional variables of the backer pad provided important information on the effect of manufacturing errors and the overall resiliency of the design. By implementing this analysis methodology on these other materials, the potential deviations can be identified prior to the expense of manufacturing. For the meta-band and backer pad, this analysis could help determine if additive manufacturing is the ideal method for their manufacturing, or if a different, more cost effective or faster method could be employed, such as an extrusion or casting method. Large scale production is not best suited for AM, therefore understanding the effects of tolerances on the design, informed decisions can be made.

More generally, these analyses could allow for the determination of acceptable ranges of deviation for meta-material designs, introducing an additional layer of feasibility checks to the overall methodology. Results could also show which variables exhibit negative interactions with each other, depending on the application of the material, and which elemental combinations and orientations are best suited to address certain considerations. Additionally, as more elements are added to the repository, their reliability

of behavior, with regards to manufacturing tolerances, can be tested and documented for designers to reference. This could help the design process run more efficiently, by allowing designers to make more informed decisions.

5.2.3. Expanded Optimization of Meta-material System

While the single level optimization technique proves most ideal in the current set-up, the bi-level method shows promise in its own methodology. The chief reason for choosing the single level over the multi-level was the difference in final ‘optimal’ results. The multi-level results were not on par with the curve matching capabilities of the single level. However, the active variables for this optimization did not include the half width of height of the unit cell. The complexity of the model was too much to manage these variable changes within the GUI, however, using a python based approach to model generation would provide the necessary control over the model to utilize these variables. By parameterizing things such as contact position, errors within the model could be eliminated and the use of a variable point of contact, relative to the model’s origin, becomes more feasible. By harnessing these previously untapped variables, combined with the implantation of size factors, the complexity of the designs increases yet again. With a larger design space and more control of the behavior, methods like the bi-level optimization may produce real and feasible designs.

Building on the use of python based model generation, this method could also allow for several different size factors to be more easily implemented in a single level. For example, having an ESG thickness use a size factor different from the size factor applied to the cantilever beam thickness in that same cell level. Yet again, this could unlock even

more control over the material behavior, and for a small tradeoff in time spent coding, could reap great benefits in the field of high performance materials and their optimization.

5.2.4. Multi-Level Optimization

For the multi-level optimization approach, additional work and modifications could increase the computational efficiency and overall success of the results obtained. Each optimization runs 50 designs per loop and, given the set-up of the optimizer, design information from previous counts of the iterative loop is not stored within the scheduler. Since the scheduler decides which combination of design variables are used in the next generation of evaluations, the possibility exists that designs are being resubmitted for evaluation. If so, this would be a waste of computational resources. The other, and more likely, possibility is that design variables well outside the range of the expected solution space are being evaluated. These are solutions that have no legitimate chance at satisfying the constraints, and therefore, should not be allocated resources for evaluation. The expectation is that the optimal variables for each material change slightly with each iteration, edging closer to the global optimal. These become the new set of fixed design variables and reset the design space as unexplored. But, slight changes in fixed variables should not legitimize designs that were comfortably above the desired constraints. By implementing a method to actively narrow the upper and lower bounds of the design variable range, less time can be committed to exploring designs that infeasible solutions. Such methods would require some further adaptations and troubleshooting of the optimization project, but it is feasible to implement.

REFERENCES

- [1] Medalia, A. I., Alesi, A. L., and Mead, J. L., 1991, "Pattern Abrasion and Other Mechanisms of Wear of Tank Track Pads," *Rubber Chem. Technology*, 65.
- [2] Dangeti, V. S., 2014, "Identifying Target Properties for the Design of Meta-Material Tank Track Pads," Clemson University.
- [3] Katz, H. S., and Wittig, J. T. J., 1986, "Development and Fabrication of Track Pads."
- [4] Ostberg, D., and Bradford, B., 2009, "Impact of Loading Distribution of Abrams Suspension on Track Performance and Durability," *Proc. 2009 Gr. Veh. Syst. Eng. Technol. Symp. Fig.*, pp. 1–11.
- [5] Mars, W. V. (Endurica L., and Ostberg, D. (U. S. A. T., 2012, "Fatigue Damage Analysis of an Elastomeric Tank Track Component," *Simulia Cust. Conf.*, pp. 1–14.
- [6] Satterfield, Z. et al., (2017). Unit Cell Synthesis for Design of Materials with Targeted Nonlinear Deformation Response. *Journal of Mechanical Design*, 139(12), p.121401. doi: 10.1115/1.4037894.
- [7] Kulkarni, Neehar Milind, (2016). "Design Optimization of Tank Track Pad Meta-Material Using the Cell Synthesis Method," Clemson University.
- [8] Kulkarni, N., Franklin, S., Fadel, G., Li, G., Coutris, N., Castanier, M., (Under Review), Modified Unit Cell Synthesis Method for Design and Sensitivity Analysis of Tank Track Pad Meta-material. *Journal of Mechanical Design*.
- [9] Satterfield, Z. T., 2015, "Design of a MetaMaterial with Targeted Nonlinear Deformation Response," Clemson University.
- [10] Morrissey, R. J., McDowell, D. L. and Nicholas, T. (1999) 'Frequency and stress

- ratio effects in high cycle fatigue of Ti-6Al-4V', *International Journal of Fatigue*, 21(7), pp. 679–685. doi: 10.1016/S0142-1123(99)00030-4.
- [11] Spierings, A. B., Herres, N., & Levy, G. (2011). Influence of the particle size distribution on surface quality and mechanical properties in AM steel parts. *Rapid Prototyping Journal*, 17(3), 195–202. Doi: 10.1108/13552541111124770
- [12] Strondl, A., Lyckfeldt, O., Brodin, H., & Ackelid, U. (2015). Characterization and Control of Powder Properties for Additive Manufacturing. *JOM*, 67(3), 549–554. Doi: 10.1007/s11837-015-1304-0
- [13] Spierings, A. B., & Wegener, M. V. T. B. K. (2015). Powder flowability characterisation methodology for powder-bed- based metal additive manufacturing. *Progress in Additive Manufacturing*. Doi: 10.1007/s40964-015-0001-4
- [14] Levy, G. Spierings, A.B., & Wegener, K. (2012). Designing Material Properties Locally with Additive Manufacturing technology SLM. *Sff Symposium 2012*, 447–455.
- [15] Farzadi, A. et al., (2014). Effect of Layer Thickness and Printing Orientation on Mechanical Properties and Dimensional Accuracy of 3D Printed Porous Samples for Bone Tissue Engineering, T. Claudepierre, ed. *PLoS ONE*, 9(9), pp. 108252. doi: 10.1371/journal.pone.0108252.
- [16] Safdar, A., He, H. Z., Wei, L., Snis, A., & Chavez de Paz, L. E. (2012). Effect of process parameters settings and thickness on surface roughness of EBM produced Ti6Al4V. *Rapid Prototyping Journal*, 18(5), 401–408. Doi: 10.1108/13552541211250391

- [17] Alharbi, N., Osman, R. & Wismeijer, D., (2016). Factors Influencing the Dimensional Accuracy of 3D-Printed Full-Coverage Dental Restorations Using Stereolithography Technology. *The International Journal of Prosthodontics*, 29(5), pp.503–510. doi: 10.11607/ijp.4835.
- [18] Hernandez, D. D. (2015). Factors Affecting Dimensional Precision of Consumer 3D Printing. *International Journal of Aviation, Aeronautics, and Aerospace*, 2(4). Doi: 10.15394/ijaaa.2015.1085
- [19] Smith, C.J. et al., 2016. Dimensional accuracy of Electron Beam Melting (EBM) additive manufacture with regard to weight optimized truss structures. *Journal of Materials Processing Technology*, 229, pp.128–138. doi: 10.1016/j.jmatprotec.2015.08.028.
- [20] Cooke A.L., Soons J.A. (2010), Variability in the geometric accuracy of additively manufactured test parts, National Institute of Standards and Technology, Gaithersburg, MD, USA. *SFF symposium*, Austin, 2010. pp. 1-12
- [21] Phadke, M. S. (2012) *Quality Engineering Using Robust Design, Technometrics*. pp. 41-67 doi: 10.1080/00401706.1991.10484810.
- [22] Dima Brockhoff, Thanh-Do Tran, Nikolaus Hansen. Benchmarking Numerical Multiobjective Optimizers Revisited. A.I. Esparcia and S. Silva. Genetic and Evolutionary Computation Conference (GECCO 2015), Jul 2015, Madrid, Spain. pp.639-646
- [23] Rosenthal, S., Rosenthal, S. and Borschbach, M. (2014) ‘Impact of Population Size and Selection within a Customized NSGA-II for Biochemical Optimization Assessed

on the Basis of the Average Cuboid Volume Indicator,” *BIOTECHNO 2014: THE SIXTH INTERNATIONAL CONFERENCE ON BIOINFORMATICS, BIOCOMPUTATIONAL SYSTEMS AND BIOTECHNOLOGIES, IARIA 2014*, pp. 1-7. doi=10.1.1.687.3218.

- [24] Migdalas, A., Pardalos, P. M. (Panos M. . and Värbrand, P. (1998) *Multilevel optimization: algorithms and applications*. Springer Publishing Company. Doi: 10.1007/978-1-4613-0307-7
- [25] McAllister, C. D. and Simpson, T. W. (2003) ‘Multidisciplinary Robust Design Optimization of an Internal Combustion Engine’, *Journal of Mechanical Design*. American Society of Mechanical Engineers, 125(1), p. 124. doi: 10.1115/1.1543978.
- [26] Maki, K., Sbragio, R. and Vlahopoulos, N. (2012) ‘System design of a wind turbine using a multi-level optimization approach’, *Renewable Energy*. Pergamon, 43, pp. 101–110. doi: 10.1016/J.RENENE.2011.11.027.
- [27] Zomorodi, A. R. and Maranas, C. D. (2012) ‘OptCom: A Multi-Level Optimization Framework for the Metabolic Modeling and Analysis of Microbial Communities’, *PLoS Computational Biology*. Edited by C. V. Rao. Public Library of Science, 8(2), p. e1002363. doi: 10.1371/journal.pcbi.1002363.
- [28] McAllister, C. D. and Simpson, T. W. (2003) ‘Multidisciplinary Robust Design Optimization of an Internal Combustion Engine’, *Journal of Mechanical Design*. American Society of Mechanical Engineers, 125(1), p. 124. doi: 10.1115/1.1543978.
- [29] “Abaqus Analysis User’s Manual Version 6.14.”